THESIS FOR THE DEGREE OF LICENTIATE OF ENGINEERING

Polymer-Based Low-Cost Micromachining of Gap Waveguide Components

SADIA FARJANA

Department of Microtechnology and Nanoscience

CHALMERS UNIVERSITY OF TECHNOLOGY

Göteborg, Sweden 2021

Polymer-Based Low-Cost Micromachining of Gap Waveguide Components

SADIA FARJANA

Technical report no MC2-442

ISSN 1652-0769

Department of Microtechnology and Nanoscience
Electronics material and Systems laboratory
Micro ans Nanosystems group
Chalmers University of Technology
SE-412 96 Göteborg
Sweden
Telephone + 46 (0)31-772 1000

Printed by Chalmers Reproservice

Göteborg, Sweden 2021

To my family

Polymer-Based Low-Cost Micromachining of Gap Waveguide Components

SADIA FARJANA
Department of Microtechnology and Nanoscience
Chalmers University of Technology

Abstract

The millimeter-wave (mmWave) and sub-millimeter-wave (sub-mmWave) frequency bands have gained significant attention over the past few years due to the growth of commercial wireless applications. As the operating frequency approaches these higher frequencies, the dimensions of the waveguide-based components continue to decrease. The decreasing feature size of those waveguide components makes the traditional machine-based (computer numerical control, CNC) fabrication method increasingly challenging in terms of time and cost, especially above 100 GHz. Additionally, this method is a serial process and cost will not scale with volume production. Micromachining has the potential of addressing the manufacturing issues of mmWave components. However, the existing microfabrication techniques either suffer from technological immaturity, are time-consuming, or lack sufficient cost-efficiency. A straightforward, fast, and low-cost fabrication method that can offer batch fabrication of waveguide components operating at mmWave and sub-mmWave frequency range is desirable to address the needs for hardware on the growing market of mmWave and sub-mmWave wireless systems.

Conventional metal waveguides have very strict fabrication requirements in terms of mechanical assembly and integration of RF electronics. In comparison, gap waveguide technology not only offers competitive loss performance but also provides several benefits in terms of assembly and integration of active components. A gap waveguide is a planar waveguide technology which does not suffer from the dielectric loss in planar waveguides and which does not require any electrical connections between the metal walls, in contrast to hollow waveguides. This thesis aims to realize gap waveguide components operating at mmWave and sub-mmWave frequency range, in a low-cost and time-efficient way by developing new polymer-based fabrication methods.

A template-based injection molding process has been designed to realize a high gain antenna operating at D band (110 -170 GHz). We can confirm that injection molding of OSTEMER is a straightforward and fast device fabrication method. In the proposed method, the time-consuming and complicated parts need to be fabricated only once and can later be reused.

A dry film photoresist-based method is also presented in this thesis to fabricate waveguide components operating between 220 - 320 GHz. Dry film photoresist offers rapid fabrication of waveguide components without using sophisticated tools. The measurement results presented in the thesis indicate that this dry film-based method is a promising method for fabricating waveguide components operating in mmWave and sub- mmWave frequency ranges.

Keywords: Antenna, Dry film photoresist, Gap waveguide, Injection molding, MEMS, mmWave, Polymer microfabrication, sub-mmWave, Waveguide.

Acknowledgements

I would like to convey my sincere thanks to my supervisor and examiner Professor Peter Enoksson, for allowing me to work under his supervision in his group. It has been a pleasure to have him as my supervisor. My greatest gratitude goes to him for his kind and thoughtful supervision, constant support, and guidance. I appreciate the responsibilities he has given me.

I would also like to thank Dr. Per Lundgren, for the technical guidance, attention, and precious time he has put in follow-up my work.

I would like to thank my co-supervisors: Dr. Sjoerd Haasl, Dr. Mohammadamir Ghaderi, and Dr. Sofia Rahiminejad for their immense time, support, and guidelines. Special thanks to Dr. Mohammadamir Ghaderi for scrutinizing the papers and for all the good advice. Thank you for always being on my side and make me feel comfortable to ask for help. My special gratitude goes to Dr. Sofia Rahiminejad for sending me immediate feedbacks, despite having stayed in a different time zone.

I am thankful to John Halonen of the Nanofabrication Lab for helping me to establish the new experimental setup in the cleanroom. Without your help, it would not have been possible. Thanks for your time, guidance, and effort. Special thanks go to all the industrial partners involved in the project, especially Thomas Emanuelsson from Gapwaves AB, Dr. Jonas Hansson from Mercene Lab AB, and Dr. Yinggang Li from Ericsson AB.

I would like to give special thanks to my colleague and friend Agin Vyas for his generous support whenever I needed his help, for helping me in the cleanroom, and for all the discussions we had about day today life. Thank you Mazhar, Azega, Qi, Carl, Vivek, Pascal for all the happy hours during our lively lunchroom discussions. I would like to thank my friend Ayesha bhabi and Tanuja apu for being by my side during all the ups and downs.

I would like to thank my parents for their continuous support and blessings. I am grateful to my mother-in-law for her blessings. I am thankful to my brothers and sister-in-law for their inspiration and love. I would like to thank my husband Shuvo for his support. Thank you for sharing your knowledge and experience and for making things a lot easier for me. Last but not least, I would like to thank my two kids, Rumysha and Affan for their love and patience.

Sadia Farjana

Göteborg, April 2021

List of Publications

This thesis is based on the work contained in the following papers:

Paper I

Sadia Farjana, Mohammadamir Ghaderi, Ashraf Uz Zaman, Sofia Rahiminejad, Thomas Eriksson, Jonas Hansson, Yinggang Li, Thomas Emanuelsson, Sjoerd Haasl, Per Lundgren, Peter Enoksson. Realizing a 140 GHz Gap Waveguide Based Array Antenna by Low-Cost Injection Molding and Micromachining. Conditionally accepted with minor revision in the Journal of Infrared, Millimeter, and Terahertz Waves.

Paper II

Sadia Farjana, Mohamad Amir Ghaderi, Sofia Rahiminejad, Sjoerd Haasl, Peter Enoksson. Dry film photoresist-based microfabrication: a new method to fabricate millimeter-wave waveguide components. Micromachines 2021, 12(3), 260.

Paper III

Sadia F., Mohammadamir G., Ashraf Uz Z., Sofia R., Per L., Peter E. Low Loss Gap Waveguide Transmission line and Transitions at 220–320 GHz Using Dry Film Micromachining. Submitted to IEEE Transactions on Components, Packaging and Manufacturing Technology.

Other related publications by the Author not included in this thesis:

S.Farjana, M.A. Ghaderi , A.U.Zaman and P.Enoksson, Polymer based D-Band Multi-layer Gap Waveguide Slot Antenna Array for Line of Sight (LOS) MIMO Systems. *ICEAA-IEEE APWC 2020, Honolulu, Hawaii, USA, August 10-14, 2020.*

S. Farjana, , Sofia Rahiminejad, Ashraf Uz Zaman, Jonas Hansson, Mohammad Amir Ghaderi, Sjoerd Haasl, Peter Enoksson , "Polymer based 140 GHz Planar Gap Waveguide Array Antenna for Line of Sight (LOS) MIMO Backhaul Links," 2019 IEEE MTT-S International Microwave Workshop Series on Advanced Materials and Processes for RF and THz Applications (IMWS-AMP), Bochum, Germany, 2019, pp. 148-150, doi: 10.1109/IMWS-AMP.2019.8880101.

Sadia Farjana, Sofia Rahiminejad, Mohammad Amir Ghaderi, Sjoerd Haasl, Peter Enoksson, Fabrication of Multilayer Planar Array Antenna by SU8. MME 2019, 30th Micromechanics and Microsystems Europe workshop. 18-20 August, 2019, Oxford, United Kingdom.

S. Farjana, A.U.Zaman, S.Rahiminejad, J. Hansson,T. Eriksson, S.Haasl, T. Emanuelsson, J. Hansryd Yinggang Li, P. Enoksson"Micromachined140 GHz Planar Gap Waveguide Array Antenna for Line of Sight (LOS) MIMO Backhaul Links" , published in Swedish Microwave day, Lund, 2018.

S. Farjana, A.U.Zaman, S.Rahiminejad, J. Hansson,T. Eriksson, S.Haasl, T. Emanuelsson, J. Hansryd Yinggang Li, P. Enoksson"Micromachined D-Band Multi-layer Gap Waveguide Slot Antenna Array for Line of Sight (LOS) MIMO Systems", published in Micronano system workshop, Finland, 2018.

Farjana Sadia, Zaman Ashraf, Enoksson, Peter. (2017). Pick and Place Assembly Technique for Fabrication of Groove Gapwaveguide Resonator. Journal of Physics: Conference Series. 922. 012017. 10.1088/1742-6596/922/1/012017.

Table of Contents

Part I

List of Figures

Acronyms

AR	Aspect Ratio
AMC	Artificial Magnetic Conductor
CNC	Computer Numerically Controlled
CPW	Coplanar Waveguides
DRIE	Deep Reactive Ion Etching
EM wave	Electromagnetic Wave
EBG	Electromagnetic Band Gap
MEMS	Micro-Electrical-Mechanical-System
mmWave	Millimeter-Wave
PCB	Printed Circuit Board
PDMS	Polydimethylsiloxane
PEB	Post Exposure Bake
PEC	Perfect Electric Conductive
PET	Polyethylene
PLB	Post Lamination Bake
PMC	Perfect Magnetic Conductive
PNA	Performance Network Analyzer
RF	Radio Frequency
SEM	Scanning Electron Microscope
SIW	Substrate Integrated Waveguide
Sub-mmWave	Sub-Millimeter-Wave
SOI	Silicon On Insulator
TE	Transverse Electric
THz	Tera Hertz
TEM	Transverse Electromagnetic
TM	Transverse Magnetic
UV	Ultraviolet
VNA	Vector Network Analyzer

Part I

Chapter 1
Introduction

Over the last decades, new generation of wireless systems have emerged, and these bring about fundamental and profound impacts on daily lives and social activities of human beings. As the radio frequency (RF) spectrum is already crowded in the lower frequency range, future wireless, telecommunication or RF applications will shift more and more to the higher frequency spectrum due to large available bandwidth, smaller component size, less interference.

The term RF refers to electromagnetic waves in the frequency range of 3 kHz to 3 THz, and therefore covers millimeter-wave (mmWave), sub-millimeter-wave (sub-mmWave) and, terahertz (THz) frequencies. The mmWaves range includes frequencies from 30 to 300 GHz, with wavelengths between 10 mm and 1 mm. On the other hand, THz, or, sub-mmWave radiation lies between 100 GHz and 3 THz (depending on the definition), which covers mmWaves and infrared light in the electromagnetic spectrum. Potential commercial wireless applications operating at mmWave and THz frequency include point to multipoint services, chip to chip high-speed links, satellite communications, automotive radars, radiometers, imaging, security systems, and biological instrumentation [1-9].

However, there are plenty of technological and mechanical challenges in designing mmWave and sub-mmWave components such as smaller size requirement, increased system density, packaging, crosstalk suppression, lower power loss dissipation, and additionally cost pressure. Some of those issues can be handled by introducing new design methodologies, new semiconductor technologies, and new integration concepts. The factors that can be addressed within the frames of the manufacturing sector are fabrication requirements needed for the realization of the delicate three-dimensional (3D) feature sizes of mmWave and sub-mmWave components in a cost-efficient scale of mass production. The well-known fact is that as long as we move towards higher frequencies the component size gets smaller. Due to this reduced size and increased sensitivity to fabrication errors, the most common serial machining techniques become unfeasible in terms of cost and manufacturing time for the application of such sub-mmWave waveguide components.

The traditional ways to fabricate waveguide components are computer numerical control (CNC) metal machining, electric discharge machining (EDM). Using these techniques to manufacture metal waveguides operating at mmWave frequencies, specifically above 60 GHz, is both complicated and costly [10-12]. The challenges become more and more prominent as the operating frequency moves towards even higher frequency, especially above 100 GHz. In this regard, having upcoming mmWave and sub-mmWave applications in mind, a new, alternative fabrication technology that can offer a low-cost, rapid manufacturing of

miniaturized waveguide components is in increasing demand. This is where MEMS (Micro-Electro-Mechanical System) based fabrication can play a significant role.

MEMS or micromachining enables the construction of 3D micro-sized structures on or within a substrate. MEMS-based sensors have been developed since the 1970s [13]. This technique relies on photolithographic processes; therefore, it produces entire batches of devices in a single run, which results in a lower cost per device when produced in volume. Hence, micromachining offers a solution to fabricate small compact components conveniently.

1.1 Waveguides and Transmission Line Technologies

Waveguides and transmission lines are the key components of any mmWave and sub-mmWave system for guiding, manipulating, or simply transmitting signals. Well-established waveguide technologies are the hollow waveguide technology, planar waveguides such as striplines, microstrip lines, coplanar waveguide (CPW), substrate integrated waveguide (SIW), and gap waveguide technology. In this section, the benefits and drawbacks of the above-mentioned technologies will be discussed.

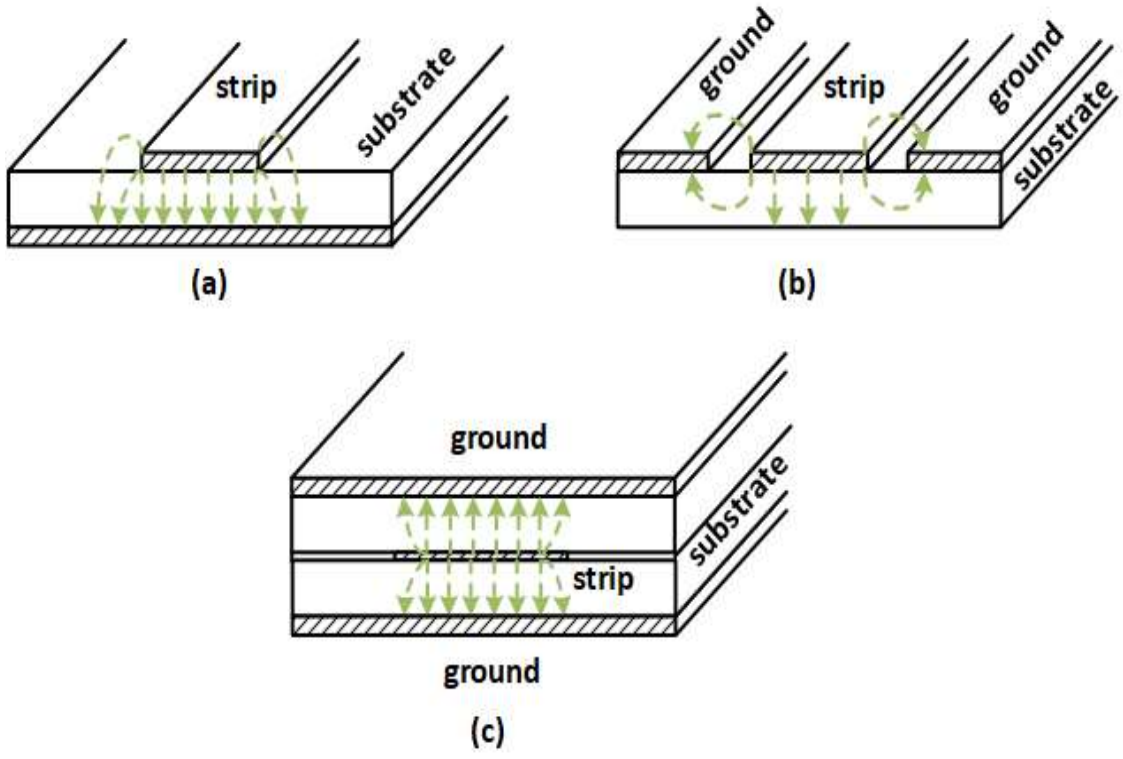

Figure 1.1: Planar transmission lines (a) Microstrip line. (b) Coplanar waveguide. (c) Stripline.

1.1.1 Planar transmission lines

The microstrip, stripline and coplanar lines are typical representations of a planar transmission line structure. Figure 1.1 shows the schematics and E-field distributions of planar transmission lines with their respective modes. The main advantages of planar transmission lines are their robustness, being mass producible at low-cost and enabling direct integration with active microwave components on circuit boards. However, these transmission lines suffer from high dielectric and ohmic losses, as the transmission property depends on material parameters of a (lossy) substrate. For this reason, these transmission lines are not suitable for high efficiency antennas and low-loss filters.

1.1.2 Hollow waveguides and substrate integrated waveguides

Standard hollow waveguides have existed in microwave operation for a long time in the form of circular waveguides, rectangular waveguides and ridge waveguides, shown in Figure 1.2. Compared to planar transmission lines, standard hollow waveguides have high power handling capability and lower losses [14]. However, their main challenge lies in finding low-cost fabrication alternatives for components in the mmWave and sub-mmWave frequency ranges. As shown in Figure. 1.2, conventional waveguides are single conductor transmission lines. If fabricated in two blocks, a very highly conductive metal connection is required between the metal blocks in order to allow propagation of the desired mode with maintained low losses. Also, the non-planar design of standard waveguides is their major disadvantage as it makes their integration difficult in the current trend of all-in-one chip integrated circuits, with passive and active components in the same module. The traditional way to manufacture standard waveguides is CNC milling and it becomes more and more challenging and expensive at mmWave frequencies [11, 12, 15].

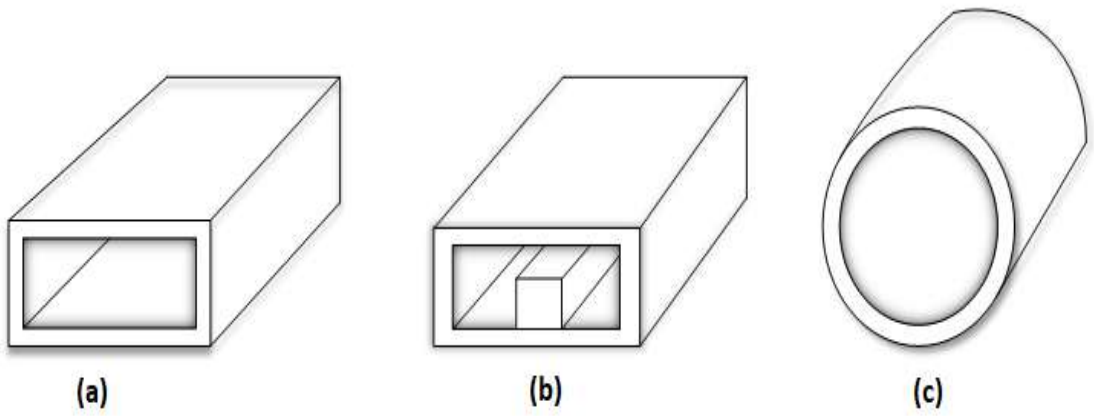

Figure 1.2: Standard hollow metal waveguide, (a) Rectangular waveguide, (b) Rectangular waveguide with a ridge, (c) Circular waveguide.

1.1.3 Substrate integrated waveguides

The substrate integrated waveguide (SIW) or post-wall waveguide, illustrated in Figure 1.3, has lately been introduced [16, 17]. It combines some of the advantages of planar transmission lines and hollow waveguides. The SIW can be realized in printed technology, where two rows of metalized via holes replace the narrow walls of the waveguide. The planar profile makes them interesting for integration with active components. However, due to the presence of a dielectric material, SIW faces the same problem as microstrip transmission lines, i.e. high dielectric losses. Also, it displays high radiation losses due to the via holes as they do not provide perfect shielding [18, 19].

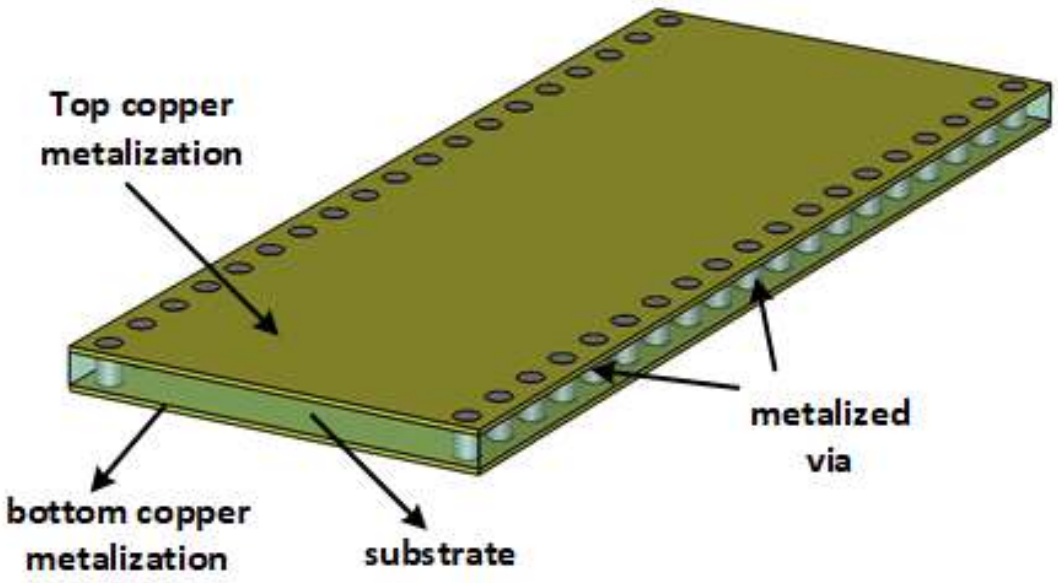

Figure 1.3: Schematic of substrate integrated waveguide.

1.1.4 Gap waveguide technology

The gap waveguide technology is comparatively new, and introduced by Kildal et Al. [20, 21]. An illustration of different gap waveguide structures is shown in Figure 1.4. In gap waveguides, the field is traveling in the air gap between parallel metal plates and unlike in a standard hollow waveguide, no connection between the side walls are required for the electrical performance of the waveguide. Moreover, like microstrip transmission lines, CPWs and SIWs, this structure can keep a planar profile, without suffering from any dielectric loss since it can support waves in the air. For these above-mentioned reasons, the gap waveguide is a promising alternative to hollow waveguides and microstrip lines for high-frequency applications. The details of gap waveguide structures will be presented in Chapter 3.

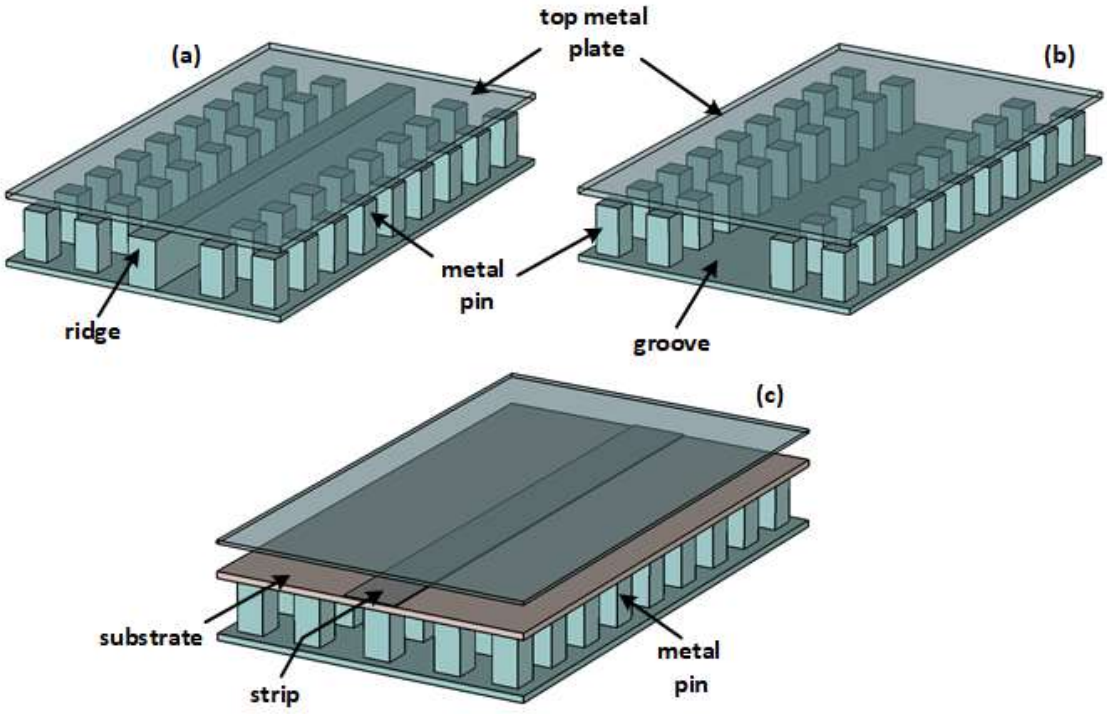

Figure 1.4: Different versions of gap waveguides. (a)Ridge gap waveguide, (b) Groove gap waveguide, (c) Microstrip gap waveguide.

1.2 Aim and Outline of the Thesis

Waveguide components operating at mmWave and sub-mmWave offer many benefits. However, the main challenge for the use of waveguide components at high frequencies comes from the wavelength-dependent miniaturization. Reduced size of the waveguide components and increased requirements on fabrication tolerances, make the conventional machining techniques impractical for the implementation of waveguide components operating at sub-mmWave. One of the major disadvantages of the milling method is as follows: it is a serial process; therefore, the production time and cost are very high for mass production. At this point micromachining has proven itself a suitable method. In the past few decades, a wide range of micromachining techniques have been proposed and developed to fabricate waveguide components operating at mmWave [22-26]. However, all the existing microfabrication techniques either suffer from some fabrication issues, or they are time-consuming, or not cost-efficient. Therefore, there is a need to develop new fabrication techniques.

Among different microfabrication methods, polymer-based methods are considered to be low-cost method. The cost of any process is a combination of production type (serial or batch), material cost, equipment cost, lab cost, and labor hours. Looking into the factors affecting the cost of any production method indicates that a fabrication method utilizing low-cost material and offering time efficient batch fabrication of devices can be claimed as a low-cost method. This thesis aims to establish such a method employing polymers.

The first part of the thesis is organized as follows:

Chapter 2 presents the current and emerging micromachining techniques used for the fabrication of waveguide components operating at and above mmWave. This chapter also presents and discusses different fabrication methods developed within the scope of this thesis.

Chapter 3 introduces gap waveguide theory, which covers an overview of the gap waveguide technology and its working principle.

Chapter 4 presents several different fabricated devices and the measurement results obtained when characterizing them.

Chapter 5 presents an overall conclusion of the thesis.

Chapter 6 presents the proposed future work that can be done.

In the second part of the thesis, the most relevant contributions of the author are included in the form of three appended papers. Additionally, other related publications can be found as references in the section List of Publications.

Chapter 2
Micromachining

In Chapter 1 we discuss the challenges of manufacturing waveguide components operating at mmWave frequencies, sub-mmWave frequencies and above. The serial nature of CNC-milled components results in high cost for volume production, which make them not affordable for most application. At this point, micromachining has proven itself a promising candidate. This chapter presents some traditional micromachining techniques used to fabricate waveguide components operating above 100 GHz. We also present the polymer-based microfabrication methods developed within the scope of this thesis.

2.1 Traditional Micromachining Techniques

Micromachining has the potential to realize small structures with great accuracy at a reduced cost. Micromachining technologies have been used in different sectors, such as the semiconductor industry, microfluidic devices, biomedical applications, sensors and actuators, and so on. The first micromachined sub-THz waveguide was manufactured in 1980 [27]. Since then different micromachining technologies have been used to fabricate sub-THz waveguide components.

Among different micromachining techniques, silicon micromachining is the well-established method. It is mostly a subtractive process in which the pattern is transferred by chemical or physical removal of the material. The first dielectric component operating at sub-mmWaves was fabricated by wet etching of a silicon wafer [27]. Later this process was used to fabricate hollow metallic waveguides [26, 28, 29]. In recent years, the deep reactive ion etching (DRIE) process has been predominantly used for manufacturing of silicon-based sub-mm components. DRIE is a bulk silicon micromachining technique based on plasma etching, where the wafer is exposed alternately to an isotropic etching plasma (sulphur hexafluoride, SF_6) and a passivation step (octafluorocyclobutane, C_4F_8) to achieve a high etch selectivity and control the side wall angle of the etched pattern. The etching and the passivation process alternate continuously until the desired depth is achieved.

The major advantage of DRIE over wet etching is its ability to deliver a high aspect ratio (AR) structure. The first silicon micromachined waveguide components by DRIE were demonstrated in 2004 [30, 31]. The DRIE process can deliver fabrication of trenches with near-vertical sidewalls and can potentially manufacture an unlimited number of structures. Additionally, the DRIE fabrication technique has very low manufacturing uncertainty, which makes it attractive

for the growing field for the fabrication of sub terahertz waveguide components. Many waveguide components fabricated by DRIE has been reported [22, 32-43].

However, the process is very time-consuming, expensive, and requires sophisticated and expensive equipment. On the other hand, multiple DRIE etches are needed to fabricate complicated structures. This technique affects the flatness of the wafer and thus the uniform resist deposition for the next DRIE process [44]. A schematic of the start and end state of a DRIE process is shown in Figure 2.1.

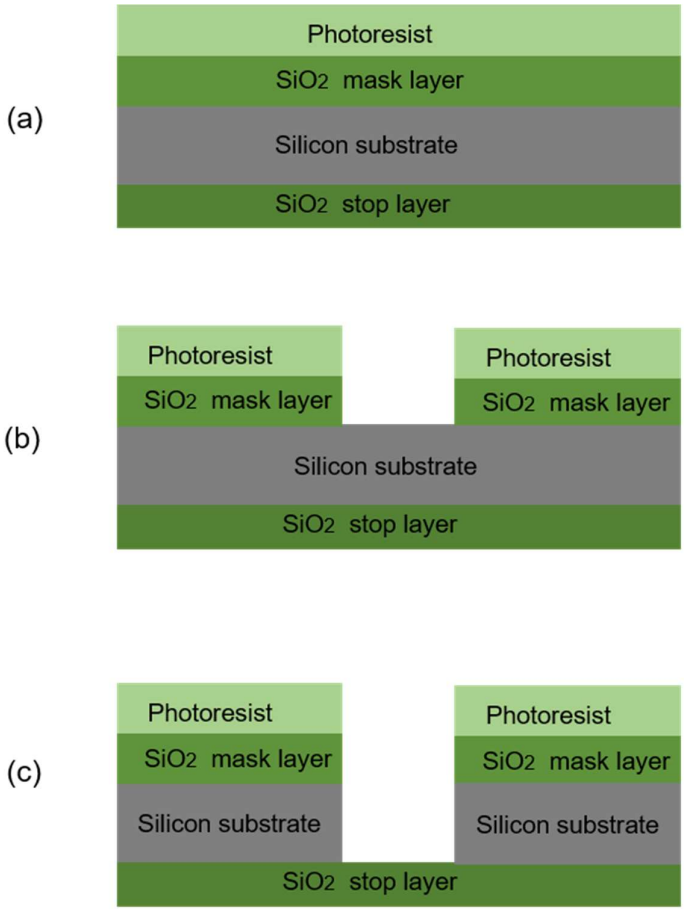

Figure 2.1: Schematic of DRIE process.

LIGA is another method to fabricated waveguide components operating at sub-mmWave. LIGA is a German acronym for lithography, electroforming, and molding developed by Forschungszentrum Karlsruhe [45]. By electrodeposition of a metal on a polymer mold, and later by dissolving this polymer mold a fully metallic structure can be obtained by this micromachining technique. Different examples of utilizing the LIGA process to fabricate the Terahertz components have been reported [46-49]. As LIGA produces metal structures it is

easier to couple to standard metal waveguide components. Still, the LIGA process has some drawbacks. This process suffers from non-uniformity issues that require an additional processing step, such as lapping, to planarize the final device. A schematic of the LIGA process is shown in Figure 2.2

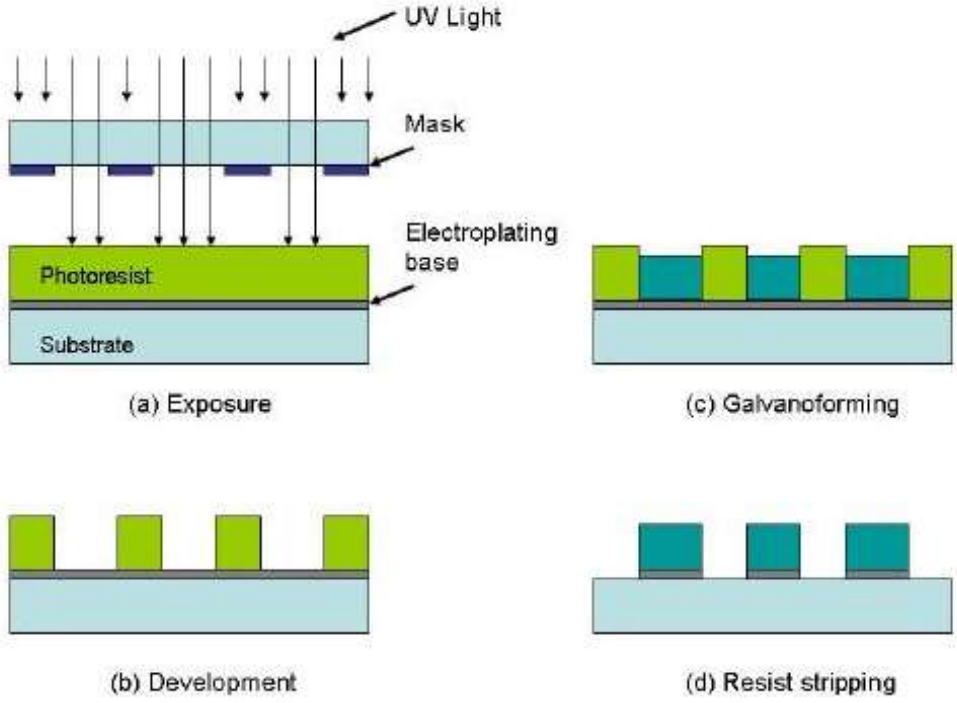

Figure 2.2: Schematic of LIGA process.

Another attractive process is to fabricate waveguide components directly from permanent photoresists. Photoresist based methods are an additive process, where layers of photoresist are spin coated, soft-baked, patterned, and coated with metal. Among other photoresists, SU8 has been used mostly to fabricate waveguide components. Many SU8 photoresist-based waveguide components have been reported [24, 25, 50-53]. SU8 is an epoxy-based negative photoresist developed by IBM in the late 80'ies [54]. SU-8 photoresist is comprised of SU-8 resin, a photo initiator, and a solvent. As a negative photoresist, the regions exposed to light become insoluble in the developer. SU8 is biocompatible, rigid, thermally, and chemically stable. Additionally, it is suitable to achieve structures of aspect ratios over 25 [55] and up to 1.5 mm high using a single coating step [56]. The main benefit of the SU8-based process is that the height of the structure is not dependent on the substrate material. By adding multiple resist layers, a thicker structure can be obtained. Also, the process does not require any sophisticated and expensive micromachining tools and thus reduces the processing cost.

However, it suffers from significant process instabilities and delamination issues between the thick resist and the carrier wafer. Additionally, while working with thick layers of photoresist, SU-8 processes are very challenging to stabilize and the layer thickness is difficult to deposit

uniformly. Moreover, the spin-coated resist layer suffers from edge bead issues and due to stress in the photoresist, the released structure suffers from a flatness problem. A schematic of the SU8 photoresist-based process is shown in Figure 2.3.

Above mentioned processes are attractive processes and bring tremendous advantages to overcome the fabrication challenges faced by traditional CNC milling. However, some works need to be done for the advancement of the microfabrication methods to fabricate waveguide components operating at mmWave and sub-mmWave.

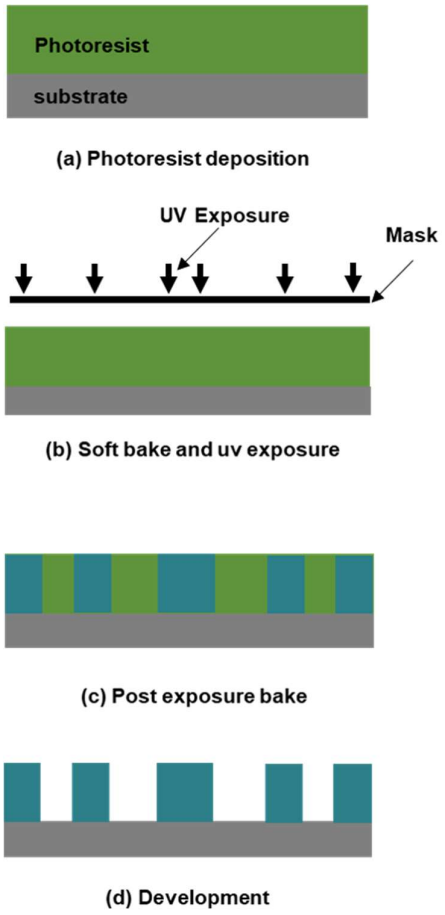

Figure 2.3: Schematic of liquid photoresist-based process.

2.2 Polymer-based Microfabrication Development

This section covers the details of the developed fabrication methods used during the fabrication of different devices presented in Chapter 4.

2.2.1 Motivation

Among different microfabrication techniques, polymer-based methods offer comparatively low-cost and straightforward fabrication processes. SU8 is the commonly used liquid photoresist that offers many attractive features. However, SU8 based processes faces several challenges mentioned in the previous section. One major issue of SU8 fabrication is flatness problem. Figure 2.4 shows a SU8-based antenna structure that is clearly buckled up due to the stress in the released SU8 films.

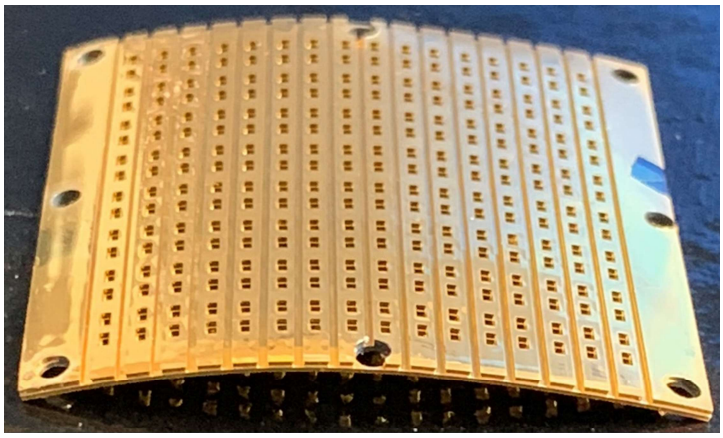

Figure 2.4: Stress-related bend in thick SU8 structure released from the substrate.

We observed, by optimizing the hard baking technique it is possible to get an optimally flat structure. In our experiment, we press the released structure in-between two wafers during the hard baking process. The hard baking was done at 165 °C for 15 mins on each side. However, if the structure contains any feature like pins then any pressure on the structure during hard baking can damage the structure. So, this is not a valid solution for all cases. Also due to the prolonged fabrication process, SU8 processing is not a suitable material for batch production.

Considering the challenges faced by SU8 fabrication method and from the need to implement new fabrication techniques two different microfabrication method have been developed in this thesis. Section 2.2.2 will present these novel microfabrication methods.

2.2.2 Methods

i) Template-based injection molding of OSTEMER

The process presented in Paper I is a combination of three main microfabrication techniques: fabricating a master by using the SU8 photoresist, fabrication of the PDMS mold, and injection molding of OSTEMER.

The master fabrication process steps involved soft bake of the thick SU8 photoresist, photolithography of the photoresist, post-exposure bake (PEB), development of the photoresist, and hard bake. To fabricate the SU8 master two different SU8 photoresists were used. SU8 2035 was used to achieve structures smaller than 110 µm and SU8 2150 was used to achieve structures greater than 110 µm. All the SU8 masters consisted of a SU8 base layer. For the base layer, SU8 2035 was used. The rest of the fabrication process was optimized for each layer, depending on their geometry, and height of the pins.

The slot array antenna has three separate layers: a slot layer, a cavity layer, and a feed layer. Each layer was fabricated in a separate process.

The slot layer was fabricated in two steps. The slot layer consists radiating slots and corrugation. The depth of the radiating slot was 750 µm and the depth of the corrugation was 490 µm. The first step was designed to obtain the slot heights until 260 µm, no corrugation was defined at this point. The remaining part of the radiating slot depth was added while defining the corrugation.

The cavity layer is comprised of cavity slots, cavity pins, and spacers to define the airgap between the cavity layer and the slot layer. The cavity slot was not considered while fabricating the cavity master. Cavity slots were later defined by the aluminum mold during injection molding. The cavity master contained only the cavity pins and the spacers. The height of the cavity pins was 644 µm and the height of the spacers was 750 µm. The fabrication was divided into two steps, where the first step defines the pins and partial height of the spacers. The next spin coat was optimized to achieve the remaining height of the spacers.

The feed layer consists of the ridge, feed pins, and spacers. The ridge had a step to provide a good impedance matching during the transition from ridge gap waveguide to WR 6.5. In the first step, the partial height of the ridge, pins and spacers were defined. Later while defining the steps the remaining height of the ridge and feed pins and the partial height of the spacers was defined. During the final spin coat, the remaining height of the spacers was defined.

Each fabrication step consisted of: deposition of SU8, soft bake, exposure, post-exposure bake. After defining all the structures required by the specific layer, the SU8 was developed and hard-baked. Later these SU8 masters were used to fabricate PDMS molds. Detailed master fabrication method was presented in Paper I. The fabricated masters are reusable.

Polydimethylsiloxane or PDMS is a commonly used elastomer in the rapid prototyping of MEMS devices because of its simple fabrication procedure. PDMS is composed of a two-parts heat-curable mixture, a polymer base, and a curing agent. Usually, the prepolymer and the curing agent are mixed in a 10:1 ratio in weight. Different mechanical properties of the final mixture can be obtained by varying this ratio. After pouring the PDMS prepolymer into the

master, the master filled with PDMS was kept in a vacuum chamber to release the trapped bubbles and later heat cured at 80°C for three hours.

Fabrication of the PDMS molds for the cavity layer and the feed layer were a straightforward process. However, the PDMS mold fabrication of the slot layer needed some process optimization. As the slot has a narrow opening, it was difficult for the thick PDMS solution to go inside the slot openings. Figure 2.5 shows the result of the heat cured PDMS mold for the slot layer. The released PDMS mold should contain pins, but the figure shows that instead of pins it formed some bubble type texture, but close inspection shows that bubbles were formed at the holes (Figure 2.5a). This is due to the trapped air bubbles due to high surface tension of the SU8. To overcome this issue, we used a toluene solution to reduce the surface tension of the SU8 structure, hence allowing the high viscosity PDMS to enter the narrow slot openings. The slot master was dipped in a toluene bath for 2 minutes and dried with a nitrogen gun, before dispensing the PDMS. Figure 2.5b shows the image of a heat cured PMDS mold after toluene treatment. Later this PDMS mold was placed together with an Aluminum (Al) mold and used for injection molding.

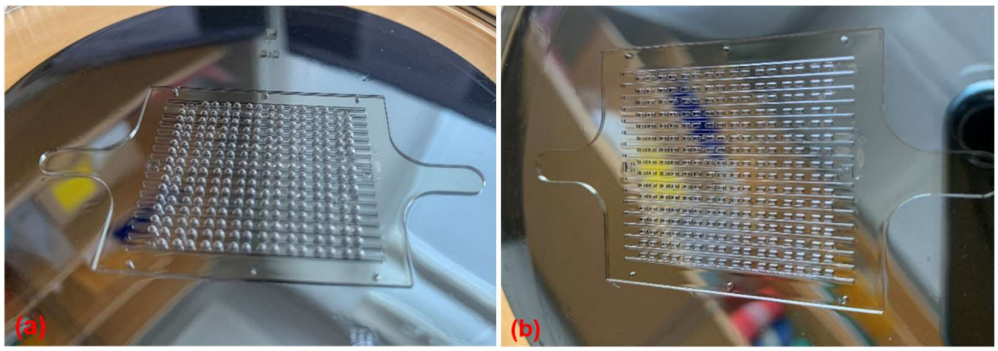

Figure 2.5: Fabrication of PDM mold for the slot layer. (a) before toluene treatment, (b) after toluene treatment.

For injection molding, Off-stoichiometry thiol–enes-epoxy (OSTEMER) polymers were used. It is a new type of thermosetting polymer developed specifically for microfabrication [57]. OSTEMER can be cured by UV exposure and later the final stiffness was given by thermal curing. The OSTEMER-based fabrication process is a straightforward process and requires minimum lab facilities [58, 59]. Process steps used during the injection molding were: aligning the PDMS mold with the respective Al mold, keep in vacuum chamber to introduce degasification effect, injecting OSTEMER pre-polymer, UV cure, release from the Al mold and, heat cure. The Al mold for the slot layer was flat as the complete structure was defined in the SU8 master and transferred to the PDMS mold. The Al mold for the cavity layer and the feed layer contained pins to define the coupling slots and opening in the feed network layer respectively. The detailed injection molding process was presented in Paper I. The pieces were then sputtered with titanium (Ti) and gold (Au) and electroplated with 1.1 µm thick Au. A schematic of the above-mentioned process is shown in Figure 2.6.

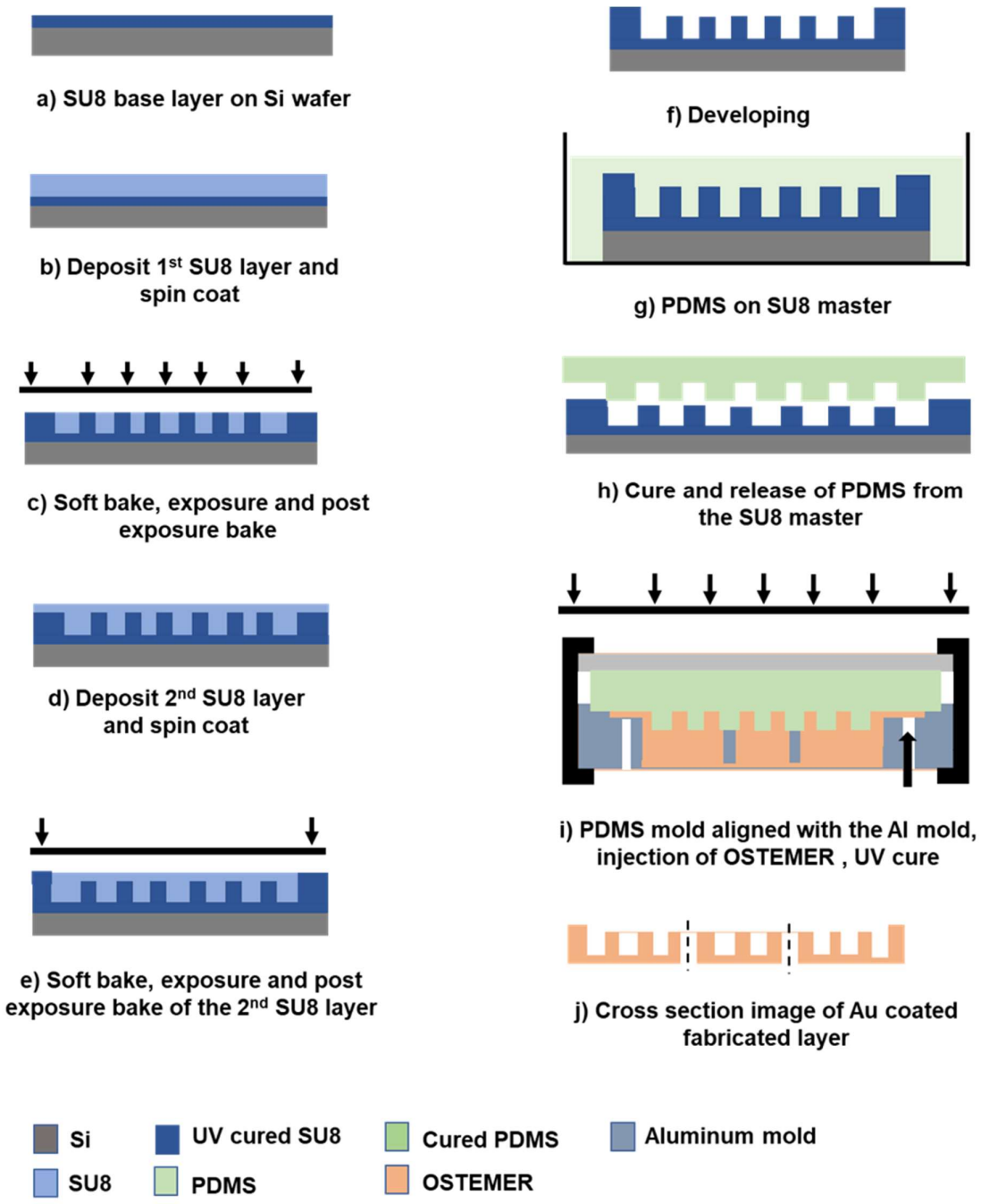

Figure 2.6: Schematic of the template-based injection molding process. (a-f) fabrication of SU8 master, (g-h) fabrication of PDMS mold, (i-j) Injection molding of polymer OSTEMER.

ii) Dry film photoresist-based method

In the process presented in Paper II and Paper III, SUEX dry film photoresist was used to obtain gap waveguide structures. Among different dry film photoresists, SUEX dry film photoresist is a suitable material to achieve high aspect ratio structures by lithography [60].

Dry film photoresists were invented almost 30 years ago and since then, have been widely used in the production of printed circuit boards (PCBs) [61]. They come as sheets of negative acting material without solvent and in pre-defined thicknesses and sandwiched between two Polyethylene (PET) sheets. The middle layer is a photosensitive layer that is initially solvable in the developer and becomes unsolvable after UV light exposure and heat treatment. Dry films are laminated on top of a substrate by hot roll lamination. Dry film photoresists have already been used for several MEMS applications and they offer many advantages over liquid photoresists [62-65]. The advantages offered by dry film photoresist are

- no edge bead,
- thickness uniformity over the whole wafer,
- fast processing,
- straight sidewalls,
- requiring less sophisticated tools
- overall lower fabrication cost

Dry film processing can be done by the following steps: lamination of the film, UV exposure, post-exposure bake, development, hard-bake. Unlike thick liquid photoresist, no prolonged soft baking is required by a dry film photoresist. Thus, the processing can be done in a very short time.

The lamination process is shown in Figure 2.7. An Al plate was used to carry the substrate during the lamination process. As mentioned before, SUEX dry film comes sandwiched between two PET sheets. Before lamination, the PET sheet from one side was removed. The rest of the PET sheet was removed just before exposing the dry-film sheet under UV light. After releasing the PET sheet of one side of the dry film it was placed on the substrate (in our case a silicon wafer). A plastic sheet was placed between the dry film sheet and the substrate and removed slowly during lamination process to assure a bubble free lamination. Another plastic sheet was used to cover the substrate during lamination to prevent any sticking with the laminator. The detail of the fabrication process is described below.

To fabricate the devices presented in Paper II and Paper III, silicon was used as a carrier and SUEX dry film was laminated on the carrier wafer as a base layer. Later three SUEX layers were laminated on this base layer that defines the pattern of the fabricated device.

A dehydration bake of the carrier is very important for better adhesion between the dry film and the silicon wafer. Even though it is not recommended to perform any post lamination bake (PLB), we used a PLB step after lamination of every SUEX sheet. The process steps to fabricate the base layer was following; lamination of thin SUEX dry film sheet, PLB, flood exposure, PEB. The schematic process steps are shown in Figure 2.8a- Figure 2.8e.

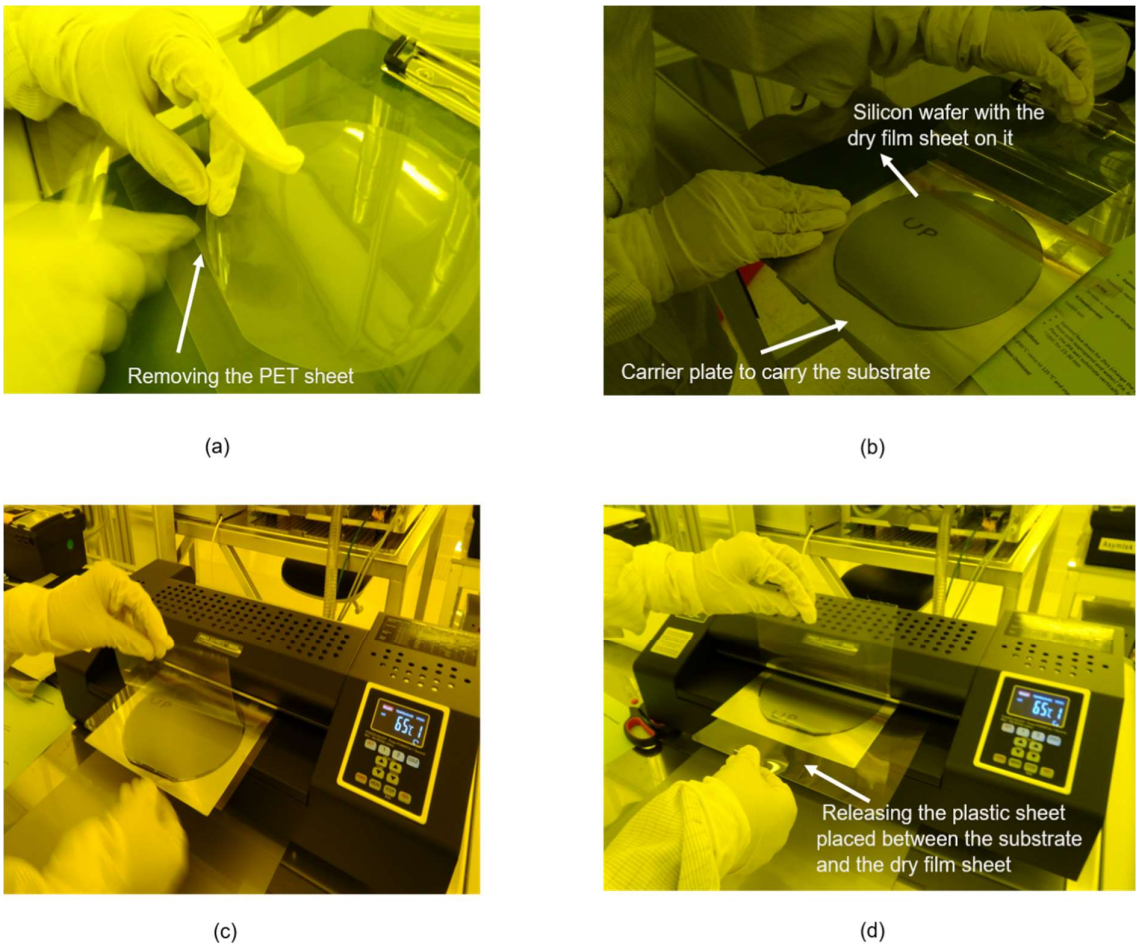

Figure 2.7: Dry film photoresist lamination steps. (a) removing the PET sheet, (b) dry film photoresist placed on a wafer and the wafer placed in carrier plate, (c) lamination of dry film photoresist, (d) withdraw the middle plastic sheet slowly.

Before laminating another dry film sheet the flood exposed layer went under a plasma ashing step to improve the adhesion of the subsequent dry film layer. To fabricate the device layer, multiple dry film sheets of different thicknesses were used. After lamination of each dry film sheet, a PLB was done. Once the laminated layers were exposed under UV with the desired mask (Figure 2.8h) it went through a PEB (Figure 2.8i). Later the whole wafer was developed. The developed wafer was directly placed on a hotplate for drying followed by hard baking. The wafer was then diced, and the chips were sputtered with a 50/900 nm Ti/Au layer. The details of the fabrication process were presented in Paper II and Paper III. A schematic of the dry film photoresist-based process is shown in Figure 2.8

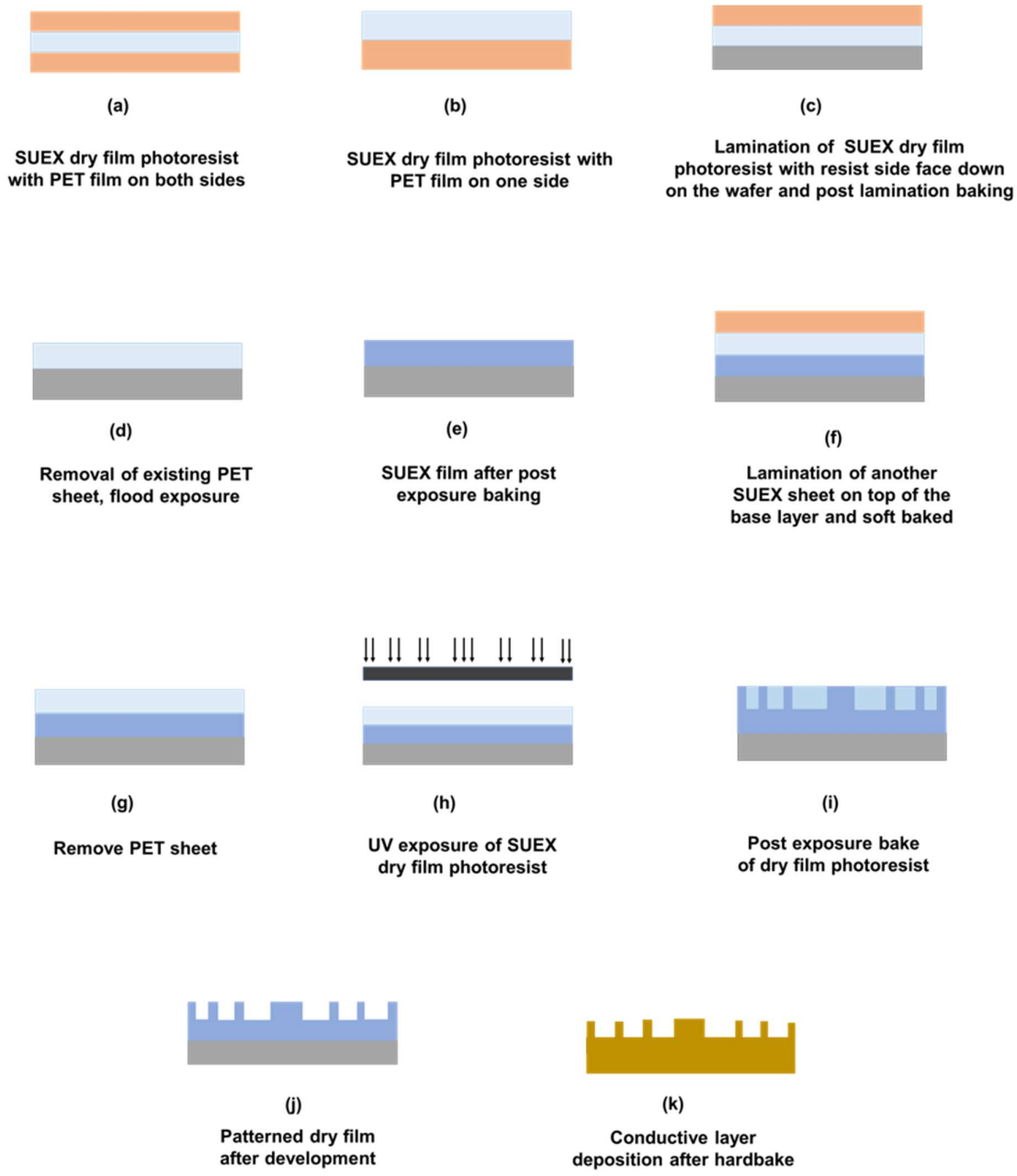

Figure 2.8: Schematic of dry film fabrication.

Process optimization

During optimization of the dry film process presented in Paper II and Paper III we noticed that exposure dose is an important parameter for SUEX dry film-based lamination process. During the fabrication process, we noticed delamination of structures during development. The effect of all the parameters such as lamination temperature and speed, PLB and PEB time, and temperature, were tested and yet the delamination issue was unaltered.

As mentioned before to fabricate the devices presented in Paper II and Paper III, three dry film sheets of different thicknesses were used to fabricate the device layer. However, during the optimization process, we started with a single dry film sheet.

The first optimization process was done to examine the adhesion quality of the fabricated SUEX structures in two different situations: one with a crosslinked SUEX base layer and another one on a bare Si wafer without a base layer. We noticed that fabricated SUEX pins showed comparatively better adhesion with a SUEX base layer. Figure 2.9 shows a microscope image of a SUEX base layer after delamination of the pins. Whereas everything was released from the wafer when there was no base layer. A 400 µm SUEX sheet and the exposure energy of 1500 mJ/cm^2 was used for this assessment. Figure 2.9b, shows the lower part of the pin has a narrow edge, which indicates the exposure dose was not sufficient to crosslink the total thickness.

The next step was to optimize the exposure dose. To optimize the exposure dose, we used a 40 µm thick SUEX sheet as a base layer and 50 µm thick SUEX sheet for the device layer. The optimized exposure dose to crosslink a 50 µm SUEX sheet was 1500mJ/cm^2.

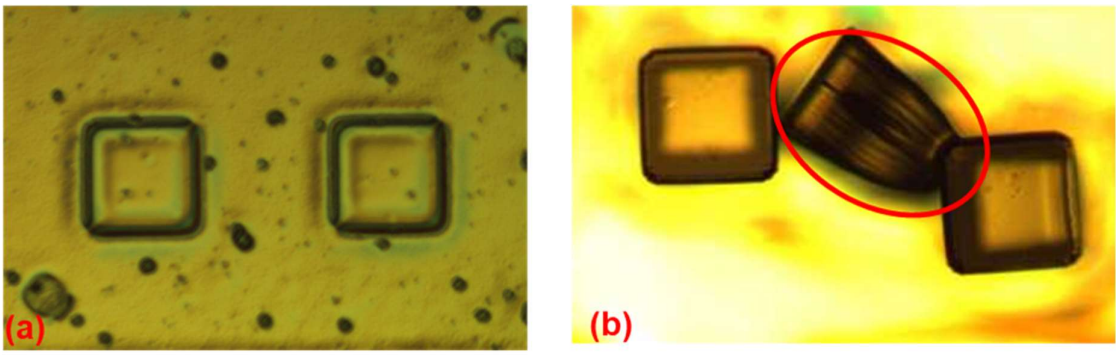

Figure 2.9: (a) Base layer after delamination of pins,(b)A pin released from the base layer.

Figure 2.10 shows a microscope image of a 50 µm thick SUEX structure where the pins are attached to the base layer. Later we optimize the exposure dose for two 50 um SUEX sheets. During optimizing three SUEX sheets of different thicknesses, we laminate the thickest layer (200 µm) first, and the thinnest layer (20 µm) last. We assume that the rate of absorption of exposure energy is higher in a thick layer than a thin layer.

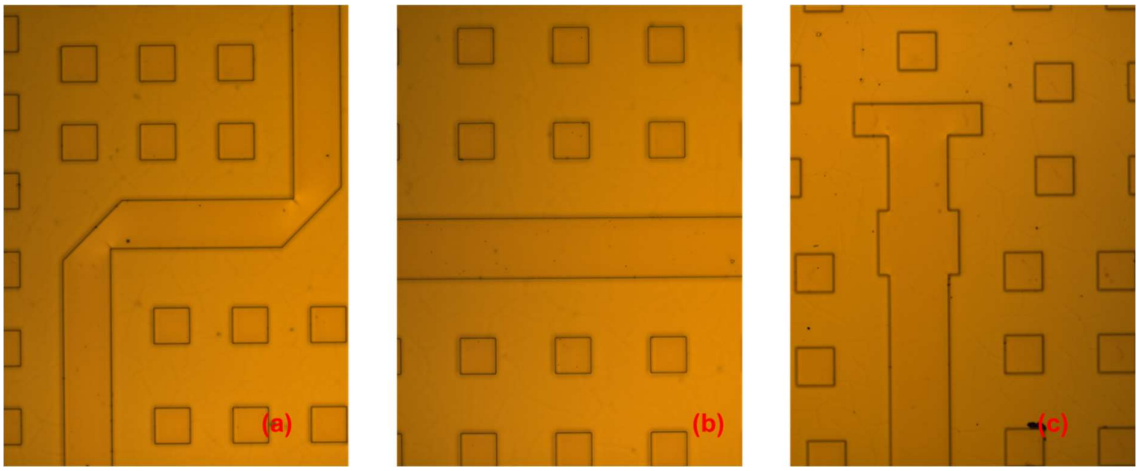

Figure 2.10: SUEX structures after optimizing the exposure dose. (a) Bend ridge, (b) Part of the resonator, (c) T- ridge section of the transition.

By optimizing the exposure dose, we were able to fabricate the gap waveguide devices presented in Paper II and Paper III. The optimized exposure doses were quite high than the recommended exposure dose mentioned in the datasheet. Table 2.1 shows optimized exposure dose of SUEX dry film photoresist for different thicknesses.

Table 2.1 shows optimized exposure dose of SUEX dry film photoresist for different thicknesses.

Dry film sheet thickness, µm	**Exposure dose, mJ/cm^2**
40	1200
50	1500
100	3000
200	6000
270	9000

Chapter 3
Overview of Gap Waveguide

The gap waveguide technology was introduced recently following the previous studies on *hard* and *soft* surfaces and the cutoff of electromagnetic waves on a parallel perfect electric conductor *(PEC)* and perfect magnetic conductor *(PMC)* waveguide configuration. [66, 67]. The gap-waveguiding concept is based on controlling the propagation of electromagnetic waves in desired directions inside a parallel-plate waveguide by using fundamentals of boundary conditions. The terms hard and soft surfaces come from acoustic theory, where, a soft surface damps the acoustic wave, and a hard surface allows propagation of the acoustic wave. In electromagnetic field theory, the PEC/PMC parallel-plate condition provides the stop surface and does not allow any propagation of mode within a certain band of interest. Similarly, the PEC/PEC configuration allows for electromagnetic wave propagation.

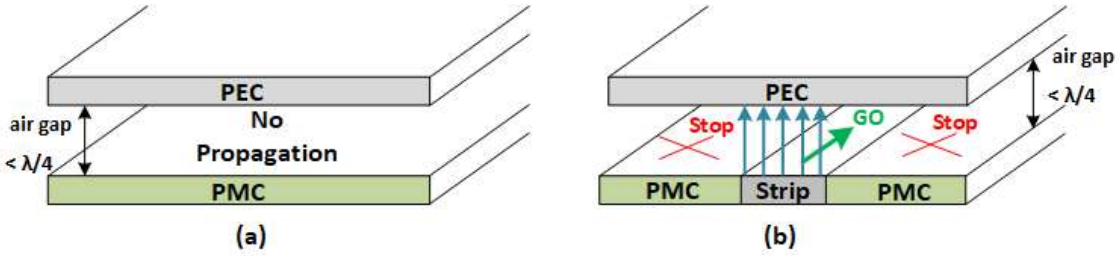

Figure 3.1: Basic concept of gap waveguide technology. (a) PEC − PMC parallel-plate electromagnetic wave cutoff. (b) TEM local waves propagation through the strip.

3.1 Fundamentals of Gap Waveguide Technology

To control the electromagnetic wave propagation, gap waveguide uses the basic cut-off of a PEC-PMC parallel-plate waveguide configuration between the two parallel plates. As long as the separation between the PEC and PMC plates is less than λ/4, no wave can propagate between the plates. But if a PEC strip is now placed on the PMC plate, the wave can propagate along the strip. The idea is shown in Figure 3.1. As PMCs are not available in nature, the PMC condition must be satisfied by artificial magnetic conductor (AMC) in the form of periodic structures such as metal pins [68] or mushroom structures [69].

An AMC surface is realized from "Fakir's Bed of Nails" [68]. To achieve a 2D AMC surface, metallic pins are arranged periodically in all directions on a conducting ground plane, shown in Figure 3.2. Over a certain frequency range, these pins create open circuit condition, resulting

in the tangential magnetic field to zero at its surface and a nonzero value for the tangential electric field. Therefore, this metallic pin-based surface acts as an AMC surface. An electrically conducting surface has the opposite characteristic. In this case, the tangential electric field is zero and the tangential magnetic field has a nonzero value.

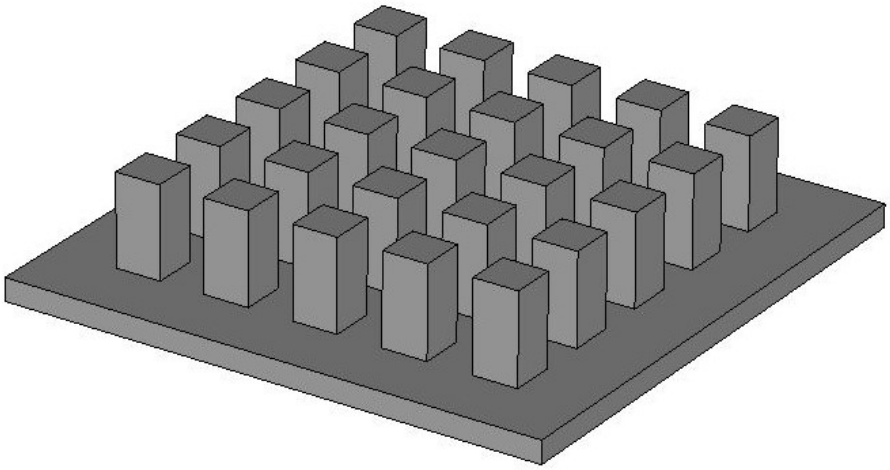

Figure 3.2: 'Bed of nails' structures by periodically placed electrical conductive pins.

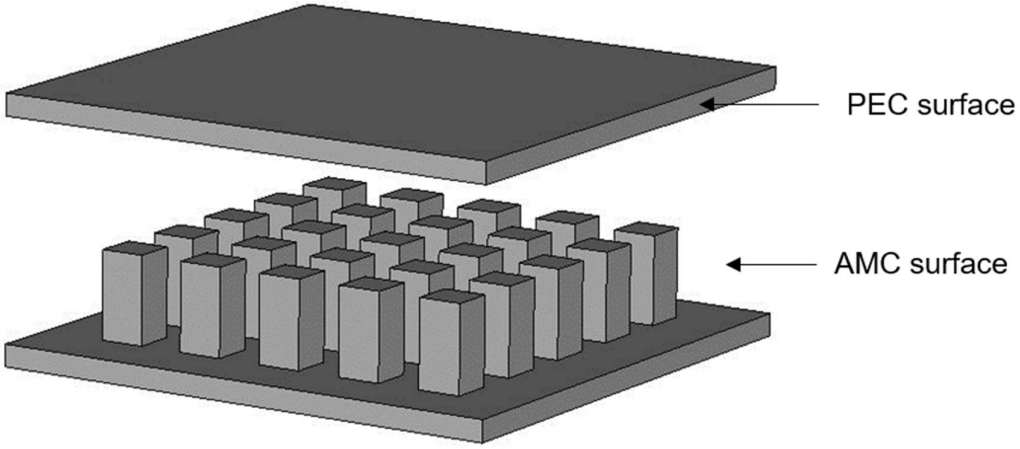

Figure 3.3: A PEC surface and an AMC surface place parallel to each other.

When a PEC surface and an AMC surface are placed opposite to each other at a short distance (preferably smaller than λ/4), due to the contradicting boundary conditions, a stopband is created, and no waves can propagate in the gap between the two surfaces [70]. Figure 3.3 shows an AMC surface and a PEC surface placed parallel to each other and this case can be referred to as an ideal parallel plate cut-off case.

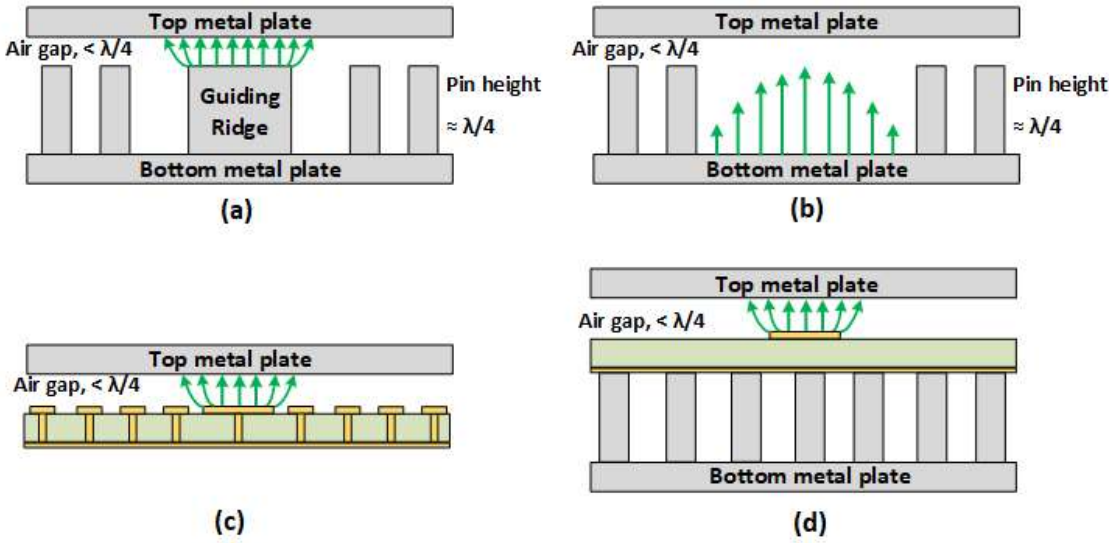

Figure 3.4: Different versions of gap waveguide geometries. (a) Ridge gap waveguide. (b) Groove gap waveguide. (c) Microstrip gap waveguide. (d) Inverted-microstrip gap waveguide [71].

Once a PEC/PMC parallel plate is formed, the addition of a metal strip in the PMC layer will allow propagation of electromagnetic waves along the strip without being leaked away in the lateral direction. The field in the two PEC/PMC regions will decay very fast. Thus, the waveguide can be formed without the need for electrical sidewalls. Based on the guiding-line, the gap waveguide can be made in different versions; strip, ridge, or groove [21, 72, 73]. Different versions of gap waveguide structures (ridge gap waveguide, groove gap waveguide, and microstrip gap waveguide) with their supported propagation mode are presented in Figure 3.4, where periodic metal pins are used as AMC surface (Figure 3.4a, Figure 3.4b, and Figure 3.4d). There are other kinds of pins that can be used to realize an AMC surface, such as the mushroom with metalized vias shown in Figure 3.4c, the inverted pyramid pin, and even a spring-shaped pin [69, 74, 75]. The propagation mode of the gap waveguide depends on the guiding structure. The ridge gap waveguide and microstrip gap waveguide both support the quasi TEM mode of propagation. On the other hand, the groove gap waveguide supports a mode very similar to the TE_{10} mode of rectangular waveguide [76].

3.2 Design of Parallel Plate Stopband Realized by Bed of Nails

As mentioned before, the periodic texture located around the ridge, groove, or strip determines the performance of the gap waveguide lines and components. Those periodic textures (e.g. pins or mushrooms) have the ability to create parallel-plate stop-band for wave propagation in the undesired direction. The geometrical parameters of the periodic structure are very important while designing the stopband to obtain the lower and upper cut-off frequency of this stopband.

A generic study and performance evaluation of different periodic electromagnetic bandgap (EBG) Structures in gap waveguide technology has been thoroughly evaluated [70]. The geometrical parameters that may influence the stopband of the parallel-plate waveguide are:

- The gap height,
- The height of the pins,
- The period of the pins,
- The radius and
- The lattice geometry.

3.3 Benefits of Gap Waveguide Technology for Sub-mmWave Applications

The gap waveguide technology covers all the benefits offered by other existing waveguide technologies. Promising features of gap waveguide structures are the planar structure, low loss, flexible manufacturing, and low manufacturing cost, especially at frequencies higher than 100 GHz. Comparing with microstrip transmission line, SIW, and CPW, gap waveguides have low loss. As the wave propagates in the air, the gap waveguide has no dielectric loss. Gap waveguide structures do not require any electrical connections between the metal walls. Therefore, comparing with hollow waveguides, it has more flexible fabrication requirements. Also, the semi-open configuration of the gap waveguide geometry gives more freedom in the integration of active electronic circuits with the low-loss metal waveguide.

As the wave propagates through the air in gap waveguide structures, they are independent of the material properties used for manufacturing. Thus, any material suitable to be used for a low-cost fabrication method can be used. The only requirement that exists in gap waveguide geometry is the metallization of the layers which has to be 4-5 times thicker than the skin depth at the frequency of operation. This introduces new opportunities to focus on batch fabrication of gap waveguide components cost-effectively.

3.4 Applications of Gap Waveguide Technology

In the previous year's gap waveguide technology has been evaluated as a useful technology and demonstrated in many different applications. The gap waveguide research was started by designing several transitions working at different frequency bands, from gap waveguide to conventional transmission lines. Several transitions between ridge gap waveguide to coaxial, CPW, microstrip line, groove gap waveguide to microstrip line and rectangular waveguide, inverted-microstrip gap waveguide to rectangular waveguide has been reported [77-83]. To determine the losses of gap waveguide structures the Q-factor of resonators can be extracted. The Q-factor of ridge gap waveguide resonator and groove gap waveguide resonators have been investigated and reported [84]. Low loss array antennas based on ridge and groove gap waveguide corporate feed network have been demonstrated [85-94]. Several researches have

been done on the microstrip gap waveguide for high-frequency array applications [95-99]. Several bandpass filters have been realized based on different varieties of gap waveguide technology. Compact bandpass filters using ridge gap waveguide, groove gap waveguide, microstrip gap waveguide, inverted-microstrip gap waveguide, and printed inverted-microstrip gap waveguide have been reported [100-113]. The gap waveguide technology represents an advantageous way of packaging high-frequency microwave circuits over the traditional packaging methods [114-116]. The gap waveguide technology has proven itself highly potential in system integration and packaging with high complexity. A Frequency-division duplex (FDD) radio front-end module has been reported, where a high-gain array antenna, a diplexer, and an RF circuit board consisting of Tx/Rx MMICs has been integrated into one single module [117].

Chapter 4
Fabricated Devices

This chapter will present the devices fabricated to verify the fabrication processes mentioned in Section 2.2.2. Some results presented in this section are repeated from the appended papers to improve the readability. The fabrication process mentioned in Section 2.2.2 (i) was used to fabricate a 140 GHz planar antenna based on gap waveguide technology. The fabrication process presented in section 2.2.2 (ii) was used to fabricate a gap waveguide-based resonator and three different low loss transmission lines.

4.1 Device Realized by Template-based Injection Molding of OSTEMER

4.1.1 Fabrication of 140 GHz slot array antenna

Paper I presents a fabrication method to fabricate a slot array antenna designed by gap waveguide technology. The antenna was designed to operate at D band. A complete 16×16 slot array antenna consists of in total, 64 sub-arrays. The antenna consists of three separate conductive layers: a slot layer, a cavity layer, and a feed layer.

The slot layer contained radiating slots and corrugation between the neighboring slot elements. The cavity layer was placed above the feeding layer and the electromagnetic energy was coupled from the feed layer to the cavity layer by the coupling slots. The feeding layer consisted of sixty-three 3-dB power dividers cascaded one after another. The dimensions of important parameters of this array geometry were mentioned in Paper I. The input reflection coefficient was measured to be below -11 dB over a 14 % bandwidth from 132-152 GHz, and the antenna gain was measured to be 31 dBi at 140 GHz, both of which are in good agreement with the simulations.

The fabrication process was discussed in Section 2.2.2. (i). The fabricated antenna is also shown in Figure 4.1. Two antennas were measured, and the measured result showed the repeatability of the process. In Paper I we presented the measurement results of similar antenna fabricated by two different fabrication methods.

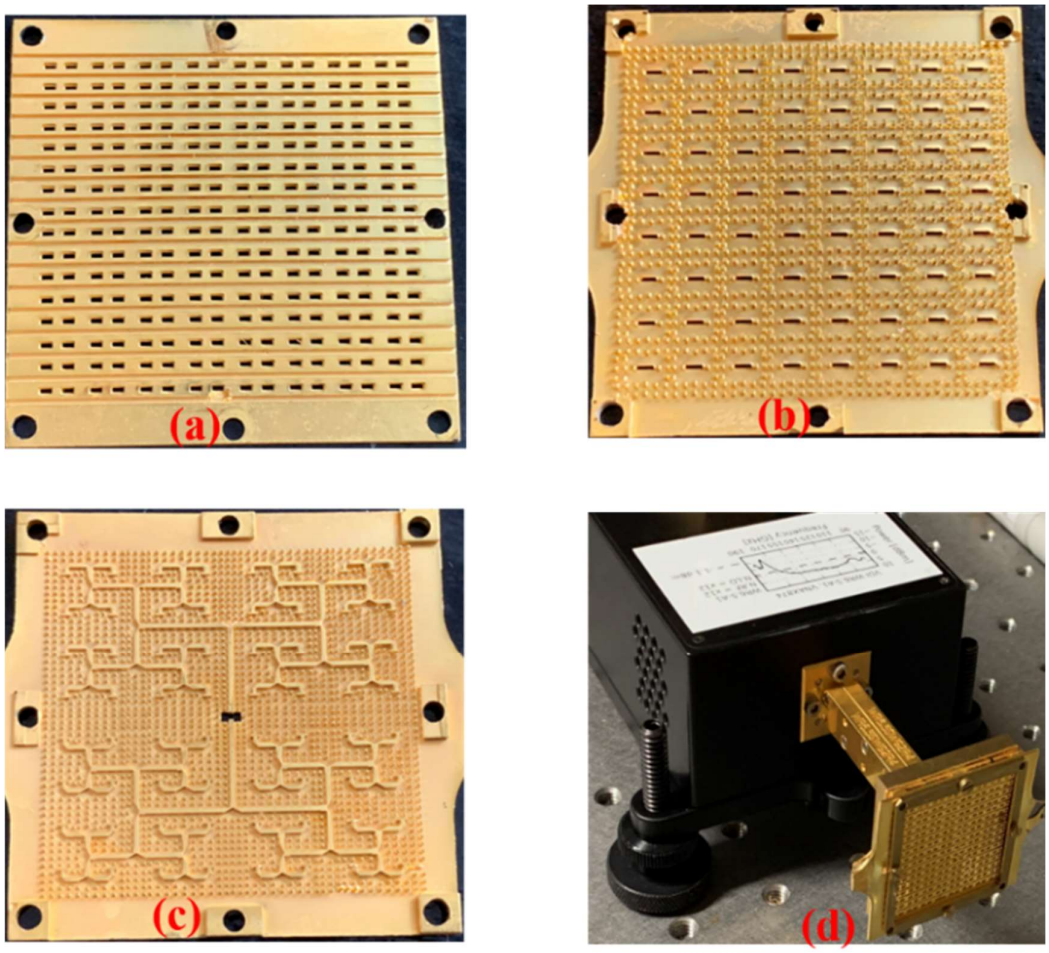

Figure 4.1: Fabricated antenna. (a) Slot Layer, (b) Feed Layer, (c) Cavity Layer, (d) Complete antenna module mounted with WR-6.5 flange.

i) Method I

In this method the slot layer was fabricated by SU8 and the cavity layer and the feed layer were fabricated by the template-based injection molding process. The geometry of the slot layer was straightforward and can be fabricated by the SU8-based method. However, the cavity layer and the feed layer have complex structures and therefore challenging to fabricated by the SU8-based method. So, we choose the template-based injection molding method to fabricate the feed layer and the cavity layer.

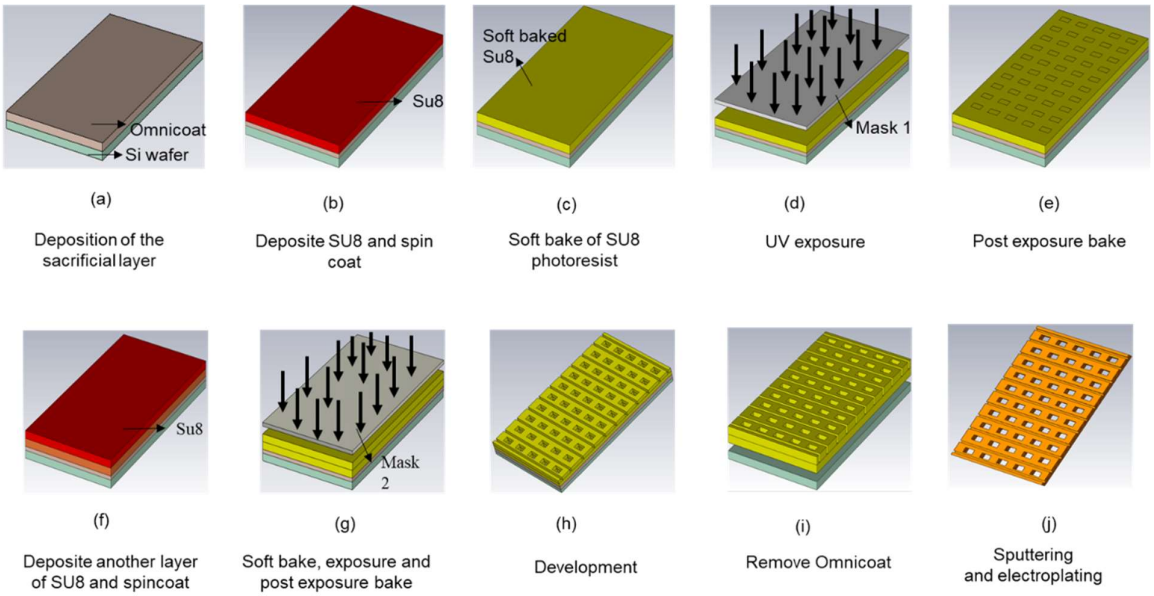

Figure 4.2: A schematic process plan to fabricate SU8 slot layer.

To fabricate the slot layer with SU8 we followed all the processing steps optimized to fabricate a slot layer master. The only additional step was depositing a sacrificial layer on the Si wafer. This sacrificial layer can be removed easily after the fabrication and the fabricated piece will be released from the wafer. We used Omnicoat as the sacrificial layer. Omnicoat was deposited on the Si wafer and spun, followed by a soft bake at 200 °C for 1 min. The rest of the fabrication process was similar to the slot layer master fabrication process mentioned in Section 2.2.2(i). Once the fabricated layer was released from the wafer a hard bake of the fabricated layer was done at 165 °C followed by sputtering of Ti and Au and electroplating of 1.1 µm thick Au to make the layer conductive. The schematic of the process is presented in Figure 4.2.

The measurement result presented in Figure 4.3 shows a peak around 145 GHz frequency in the reflection coefficient of the prototypes. The peak in S_{11} at 145 GHz can occur as a result of impedance variation in the feed line due to misalignment among all the antenna layers. Different shrinkage rates of different materials could be a reason for this misalignment. SU8 does not shrink during curing while PDMS is known to shrink during curing. Therefore, there were some misalignment between the slot layer, the cavity layer, and the feed layer even though we compensated for PDMS shrinkage. As these variations are random process variations, the only way to avoid these is to optimize the fabrication process to minimize the misalignments.

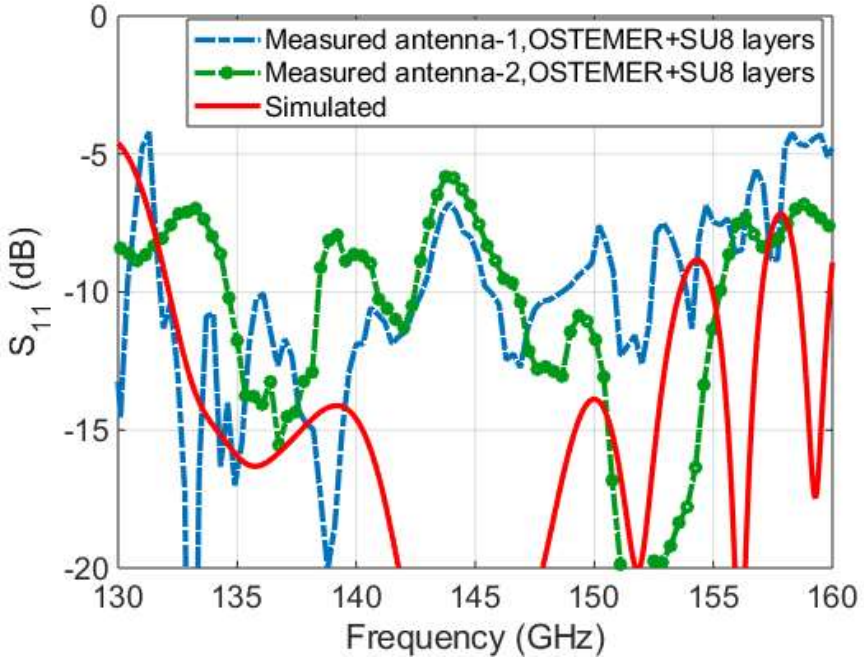

Figure 4.3: Simulated and measured S_{11} for the 16×16 element antenna array. Slot layer was made of SU8, the cavity layer, and the feed layer was made of OSTEMER.

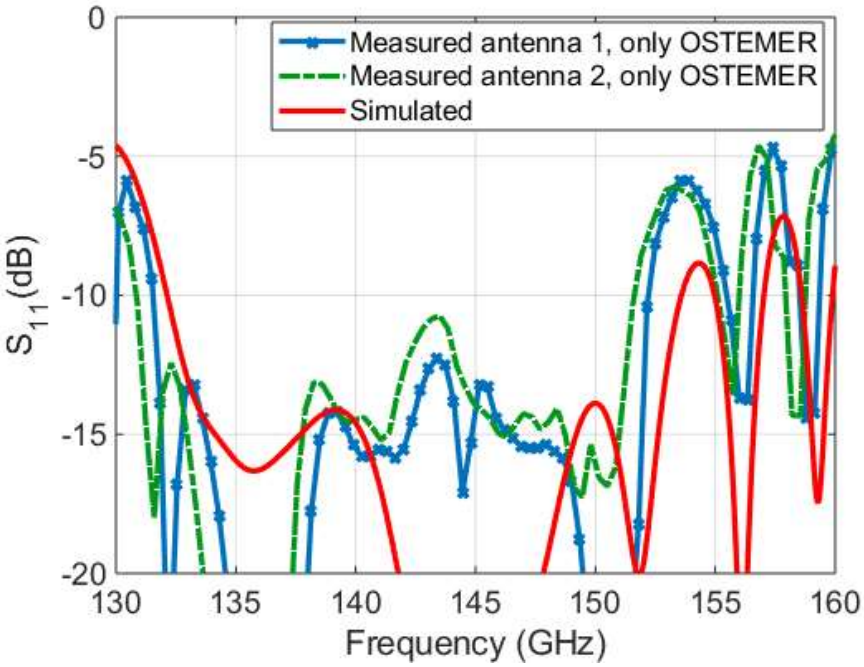

Figure 4.4: Simulated and measured S_{11} for the 16×16 element antenna array. All layers were made of OSTEMER.

ii) Method II

To overcome the complications introduced by different layers being made of different materials, we fabricate all three layers by template-based injection molding. Figure 4.4 shows that the antenna's S_{11} performance has been improved over the band 132-152 GHz by changing the fabrication process. The simulated S_{11} for the complete 16×16 element antenna array is well below -11 dB level over the band of interest, 135-150 GHz. The radiation pattern and the gain of the array antenna fabricated by method II, were measured in an anechoic chamber. The simulated and measured radiation patterns are presented in Paper I and the measured patterns showed a good agreement with the simulated patterns.

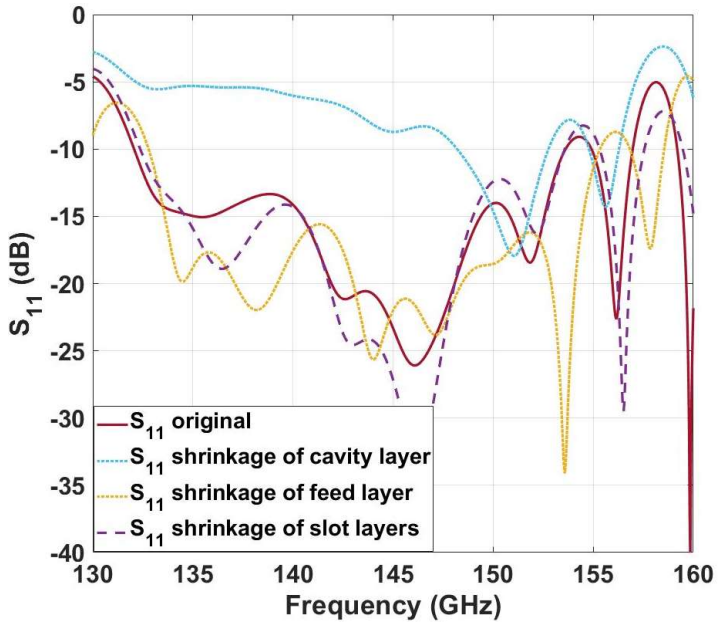

Figure 4.5: Simulation results showing the shrinkage effect of a single layer.

4.1.2 Discussion

The improved S_{11} indicated that a reduction in the misalignment between layers improves the performance.

However, there were some issues left that affected the antenna S_{11} performance.

1) PDMS shrinkage compensation error.
2) Alignment error between the PDMS mold and aluminum mold for the cavity layer and the feed layer.
3) Alignment error while mounting all three layers in the base plate.

These issues are discussed below. The effect of shrinkage on one specific layer was investigated by using CST microwave studio. Figure 4.5 shows the effect of shrinkage on each layer on the antennas S_{11} performance. The results show that the shrinkage of the cavity layer while the rest of the layers remain at original size, has the most destructive effect on the performance of the antenna. Another simulation was also conducted to understand the effect of similar shrinkage or expansion on all three layers. Figure 4.6 shows when all layers experience a similar amount of shrinkage or elongation compare to the optimized antenna dimensions, the operational bandwidth of the antenna shifts towards higher frequency or lower frequency respectively. Calculated PDMS shrinkage was 1.4 ± 0.1%. This indicates that the calculated PDMS shrinkage measurement error was approximately ± 32 µm over the total dimension of each layer. As Figure 4.4 shows that the S_{11} has slightly shifted towards lower frequency, thus we assume the PDMS shrinkage was somewhat overcompensated.

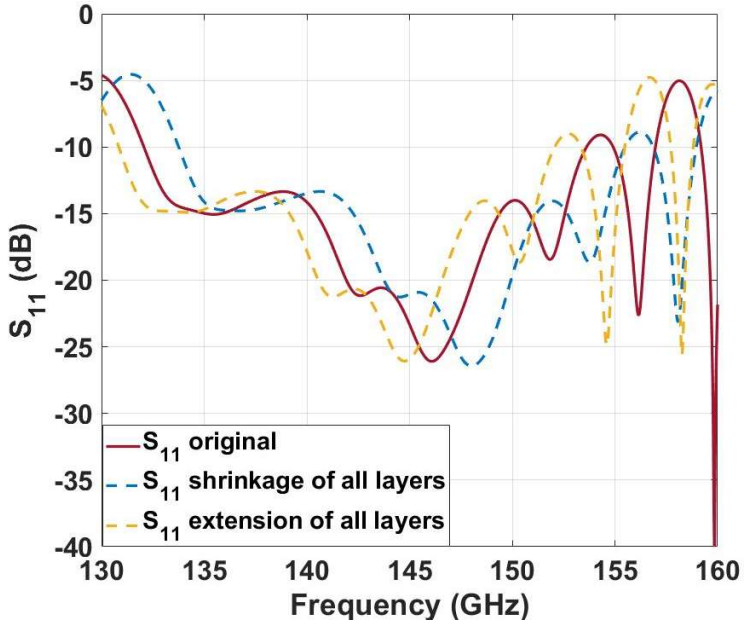

Figure 4.6: Simulation results showing the shrinkage effect and expansion effect, when all layers experience similar shrinkage or similar expansion.

Another misalignment was introduced between the cavity PDMS mold and the cavity Al mold. As mentioned earlier partial structure of the cavity layer was fabricated by the cavity master. The remaining part of the cavity layer was transferred by the Al mold. To fabricate the complete cavity layer, the PDMS mold and the Al mold needed to be placed together. This was a manual process, which might introduce some misalignment. On the other hand, the PDMS shrinkage calculation error which was approximately ± 32 µm introduces some alignment error between the cavity pins and cavity openings. The misalignment between the cavity PDMS mold and the cavity Al mold is presented in Figure 4.7. Additionally, during measurement, three fabricated layers were placed on a base plate with the help of four guiding pins and four screws. Those guiding pins and mounting screws can introduce some rotational error among the layers.

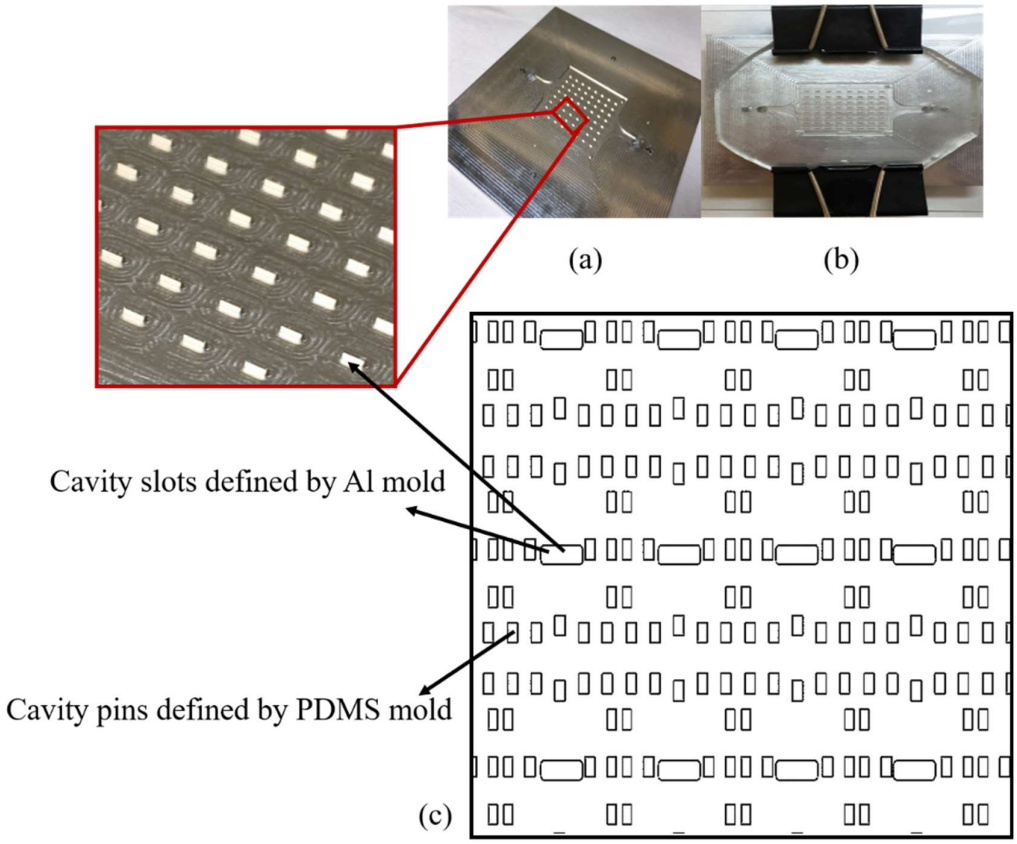

Figure 4.7: Misalignment between PDMS mold and Aluminum mold. (a) aluminum mold for the cavity layer, (b) placing PDMS mold with the aluminum mold for injection molding of OSTEMER, (c) schematic of misalignment that happened during placing two molds

4.2 Devices Realized by Dry Film Photoresist-based Method

4.2.1 Fabricated devices

i) Gap waveguide resonator

Paper II presents a ridge gap waveguide resonator to exhibit two resonances at 234.6 GHz and 284 GHz. The height of the ridge and the pins is 270 µm. The fabricated resonator is presented in Figure 4.8. The fabrication process is described in Section 2.2.2. (ii). Detail of the fabrication process can be found on Paper II. The pin height of the fabricated device was measured 272 ± 2 µm which compared to the target thickness of 270 µm exhibit an excellent height uniformity and flatness over the laminated area. The SEM image presented in Figure 4.8 shows that the sidewalls have a high verticality.

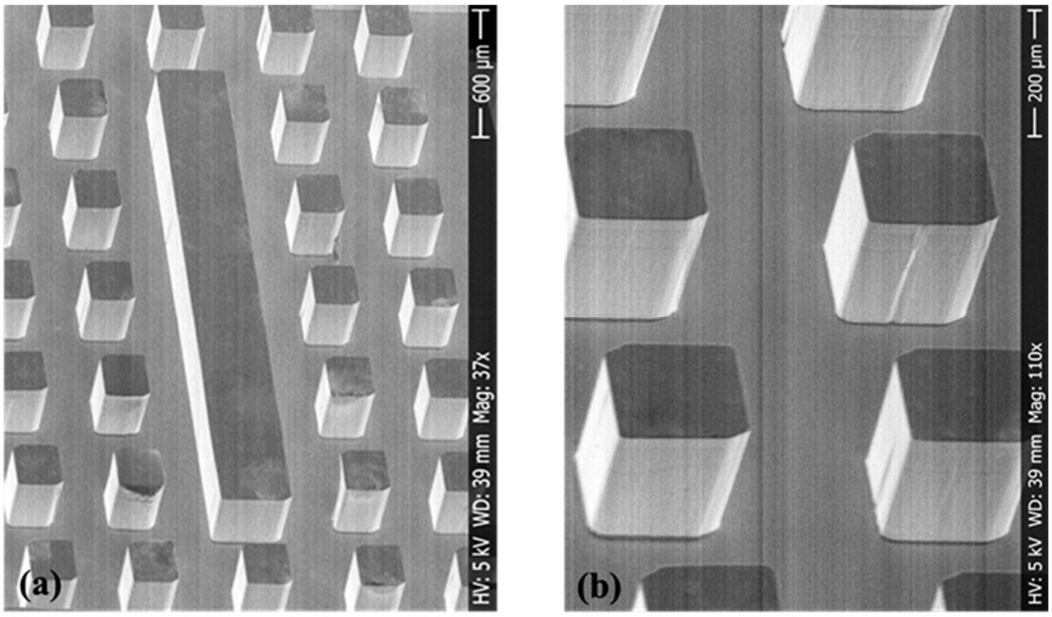

Figure 4.8: (a)SEM image of SUEX ridge gap resonator, with a pin height of 270 µm, (b) closed view of the pins of SUEX ridge gap resonator.

The unloaded Q-factor of the resonator is obtained by using the following equations [14, 84],

$$\frac{1}{Q_L} = \frac{1}{Q_U} + \frac{1}{Q_E} \qquad (1)$$

$$Q_U = \frac{Q_L}{1 - S_{21}} \quad (2)$$

$$Q_L = \frac{f_o}{\Delta f_{3d}} \quad (3)$$

$$Q_E = 10^{-[S_{21}(dB)/20]} \cdot Q_L \quad (4)$$

$$\alpha = \frac{\beta}{2Q_U} \quad (5)$$

where Q_L is the loaded Q-factor, Q_U is the unloaded Q-factor, Q_E is the external Q-factor (due to the loading effect), f_o is the resonance frequency, Δf_{3dB} is the 3-dB bandwidth of the resonance. The attenuation constant can also be extracted from the unloaded Q-values by using equation (5)

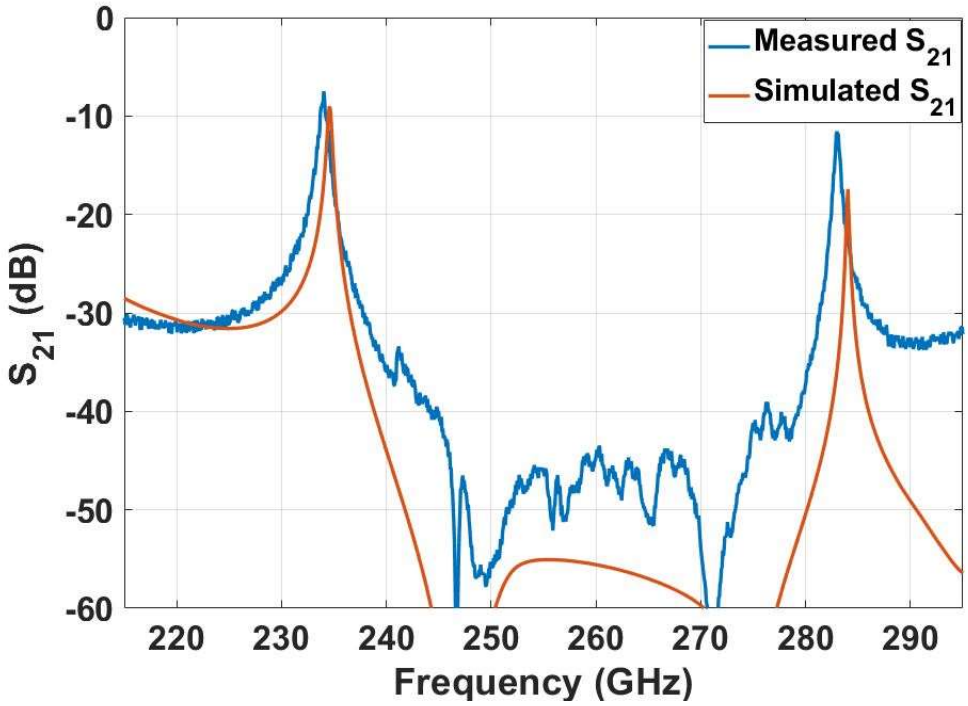

Figure 4.9: Full electromagnetic wave simulation compared with measurement results between 220 and 320 GHz. The two resonant frequencies are around 234 GHz and 283 GHz.

The measurement result was presented in paper II as well as in Figure 4.9. Table I shows the calculated unloaded Q-values, and the corresponding loss/mm from the simulations. The loss was calculated with equation 5.

Table I: Measured unloaded Q-values and corresponding loss/mm for the SUEX dry film ridge gap resonator.

Parameters	**Simulated**		**Measured**	
Frequency (GHz)	234.6	284	234	283
Q_u-value	802	938	656	786
Loss (dB/mm)	0.026	0.028	0.032	0.033

ii) Gap waveguide transition

Paper III presents three different gap waveguide transmission lines and transitions. As mentioned in Chapter 3, the guiding structure in the gap waveguide structure can be either ridge or groove. Two different types of ridge structure; straight ridge line and bend ridge line with two 90-degree bends, and a groove gap line have been designed, fabricated, and demonstrated. The paper also presents zero step transition between a rectangular waveguide to a gap waveguide. The designed and demonstrated transitions are wide band. The significances of the designed transitions are their simplicity, easy assembly, high tolerance to manufacturing and assembly error, and wideband performance. Figure 4.10 shows the three fabricated chips. For all these transitions, the waveguide port was located on top of the metal plate of the waveguide. This top plate acts as the PEC surface of the gap waveguide structures and the rows of pins on the bottom plate acts as a PMC surface. Details of the designed transitions were presented in Paper III.

To facilitate the measurement, three different support packages were designed and manufactured by CNC milling for three fabricated chips. The top part of the support package has the opening for the standard WR-3.4 rectangular waveguide. This top plate also acted as a PEC surface during the measurement. The bottom part of the support package has a channel for the chip. The channel was designed in a way, so the chip did not move during the measurement. Figure 4.11 shows the image of a support package containing the chip in its position.

The measurement results are presented in Figure 4.12, Figure 4.13, and Figure 4.14. Measured insertion loss for all three fabricated devices are presented in Table II.

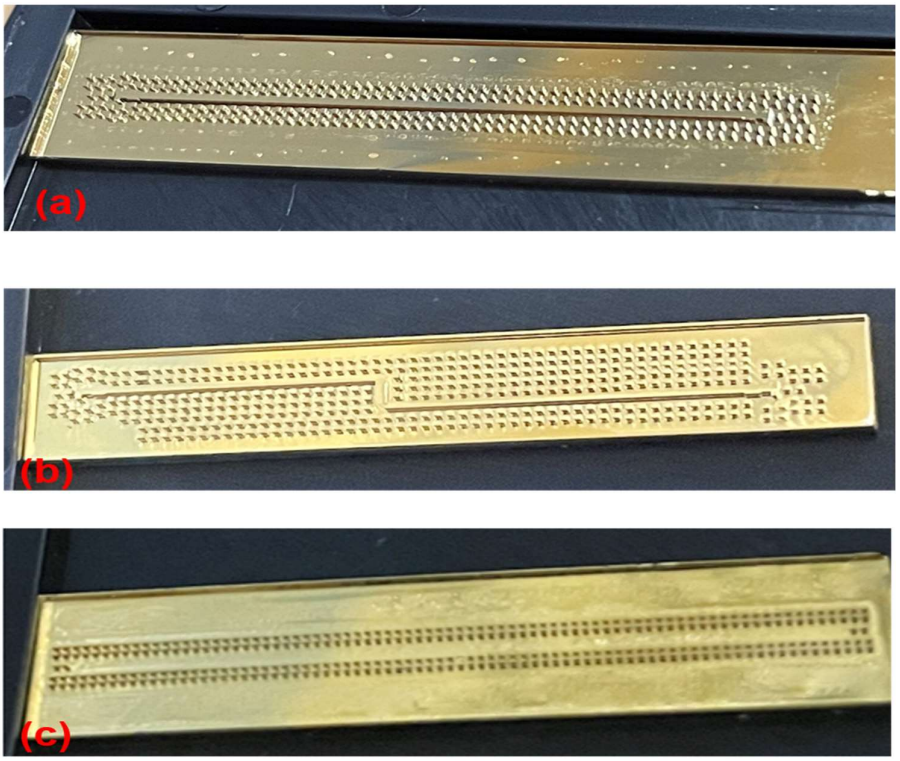

Figure 4.10: Fabricated chip. (a) Straight ridge gap waveguide (b) Bend ridge gap waveguide, (C) Groove gap waveguide.

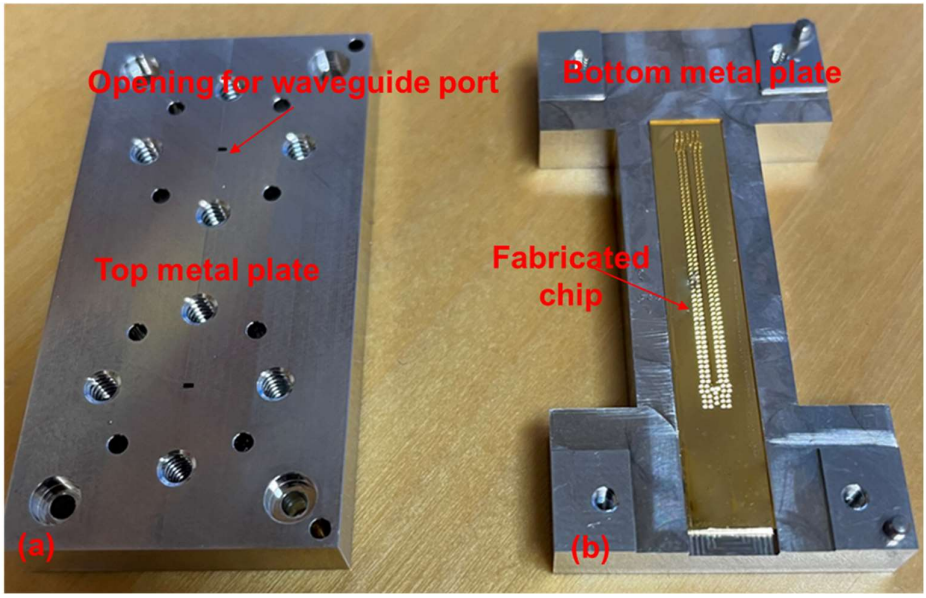

Figure 4.11 (a)Top plate of the support package with the opening for waveguide flanges, (b) bottom plate with the chip placed in the designed channel.

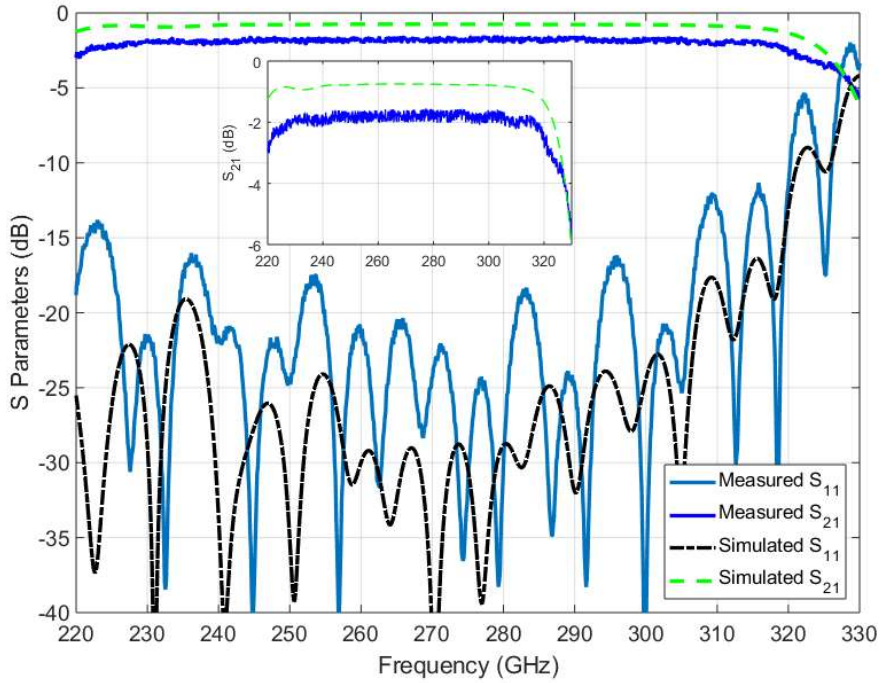

Figure 4.12: Simulated and measured S-parameters for straight ridge gap waveguide to rectangular waveguide transition.

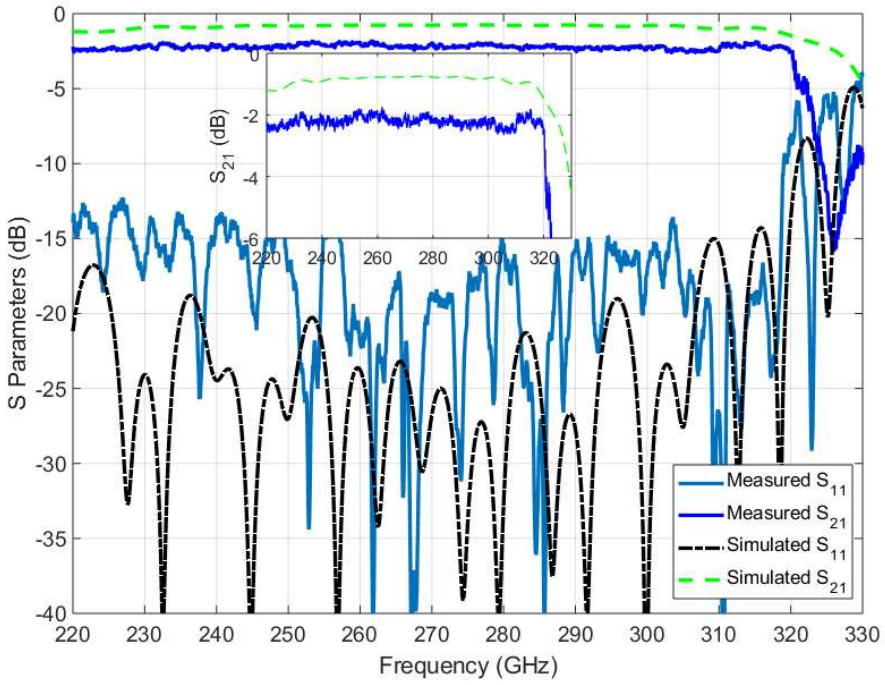

Figure 4.13: Simulated and measured S-parameters for bend ridge gap waveguide to rectangular waveguide transition.

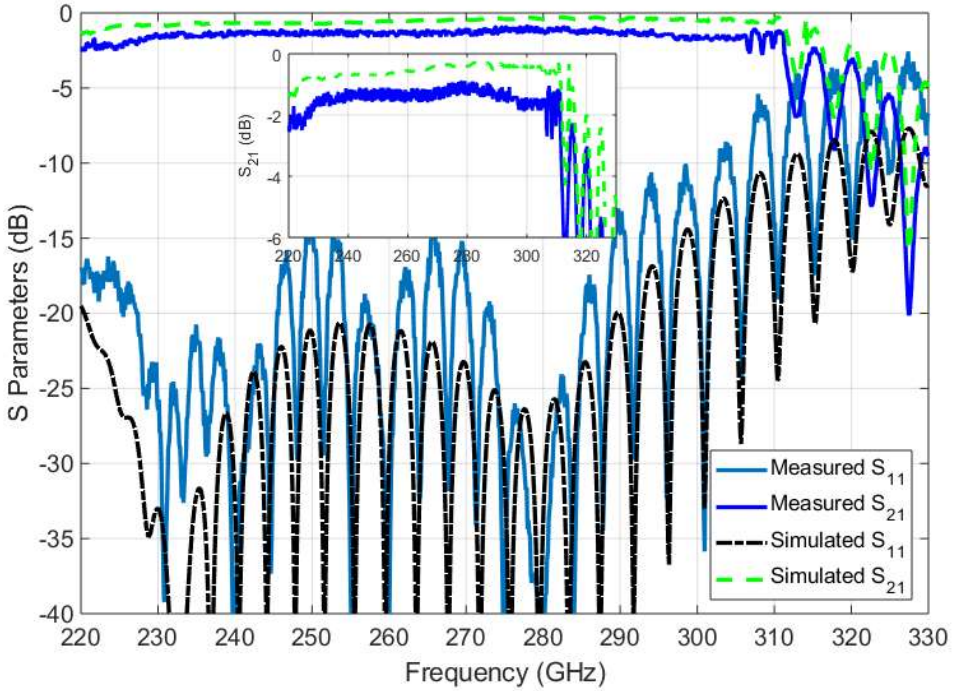

Figure 4.14: Simulated and measured S-parameters for groove gap waveguide to rectangular waveguide transition.

Table II: Measured insertion loss of straight ridge gap waveguide transition, bend ridge gap waveguide transition, groove gap waveguide transition

Device	Frequency (GHz)	Loss(dB/mm)
Dry film photoresist Straight RGW-RW	220–320	0.07-0.08 Average: 0.075
Dry film photoresist Bend RGW-RW	220–320	0.07-0.085 Average: 0.078
Dry film photoresist GGW-RW	220–320	0.02-0.07 Average: 0.048

Chapter 5
Discussion and Conclusion

At mmWave and sub-mmWave frequencies the traditional machine-based waveguide manufacturing method becomes costly, laborious and challenging. Micromachining processes proved themselves suitable at these frequencies. However, the existing micromachining techniques suffers from some fabrication issues and need to be optimized for the waveguide components operating at mmWave and sub-mmWave. Additionally, those methods put an adverse effect on the production cost due to their prolonged and complicated fabrication process. Also, in many cases they require very sophisticated fabrication tools and fabrication environment. At this point, a time efficient and low-cost fabrication method that can fabricate waveguide components operating at and above sub-mmWave will be valued highly by the wireless industry.

Gap waveguide technology, on the other hand, is a promising waveguide technology. It offers several benefits over the existing planar waveguides and hollow waveguides. The attractive feature of gap waveguides is that the electromagnetic wave propagates through air in the gap waveguide structures. Thus, the waveguide is independent of the material properties used for manufacturing. Therefore, any material suitable to be used for low cost fabrication can be used for fabrication of gap waveguide structures. This introduces new opportunities to focus on batch fabrication of gap waveguide components in a cost-effective way.

The presented template-based injection molding process presented in this work shows a rapid manufacturing method. By taking the advantages of existing SU8-microfabrication method, the template-based injection molding fabrication method was designed. The fabricated SU8 master and PDMS mold are reusable and will thus reduce the fabrication time. The final device is then fabricated by injection molding of photoresist OSTEMER. The validity of the designed fabrication process was investigated by fabricating a high gain slot array antenna. The measurement result shows good agreement with the simulation results. This rapid, straightforward, and novel fabrication method successfully demonstrated a high gain antenna. However, as the alignment between two molds were done manually, the template-based injection molding process suffers from alignment mismatch. The automation of the alignment process can reduce the alignment error.

Another micromachined fabrication method presented in this thesis is based on dry film photoresist. Dry film photoresist-based fabrication proves to be a promising method to fabricate waveguide components operating at sub-mmWave frequencies. This process overcomes many challenges faced by commonly used liquid photoresists. This process not only can fabricate waveguide components with high accuracy, but also reduce the fabrication time and complexity.

Different gap waveguide devices have been demonstrated by a dry film photoresist fabrication method. Promising measurement results of the dry film-based devices opens a new door towards low-cost waveguide component fabrication at mmWave and sub-mmWave frequency range.

Chapter 6
Future Work

There are many things that need to be done to validate the presented fabrication methods. Different devices focused on different application can be demonstrated by the newly developed fabrication methods, to investigate if the requirement can be fulfilled by the fabricated devices.

So far, the template-based injection molding process has been used to demonstrate a D-band antenna and the dry film-based process used to demonstrate the waveguide components operating from 220 to 320 GHz. Waveguide components operating above 300 GHz can be fabricated to investigate the performance of the fabricated devices.

Filters are very sensitive to fabrication accuracy. Diplexer and band pass filter can be demonstrated to investigate the fabrication method performance.

Integration of waveguide components are a challenge for sub-mmWave components. The fabrication methods can be investigated for integration purpose.

Dry film photoresist can be investigated to fabricate different structures such as double-sided structure, overhang structures and structures with different height.

Testing the effect of temperature fluctuation on OSTEMER and SUEX dry film photoresist can be interesting aspect to investigate. Thermal shock testing and temperature cycling testing can be done to realize the effect of temperature on those materials.

Bibliography

1. Lockie, D. and D. Peck, *High-data-rate millimeter-wave radios.* IEEE Microwave Magazine, 2009. **10**(5): p. 75-83.
2. Hasch, J., et al., *Millimeter-Wave Technology for Automotive Radar Sensors in the 77 GHz Frequency Band.* IEEE Transactions on Microwave Theory and Techniques, 2012. **60**(3): p. 845-860.
3. Ou, Y. and G.M. Rebeiz, *On-Chip Slot-Ring and High-Gain Horn Antennas for Millimeter-Wave Wafer-Scale Silicon Systems.* IEEE Transactions on Microwave Theory and Techniques, 2011. **59**(8): p. 1963-1972.
4. Waters, J.W., et al., *The Earth observing system microwave limb sounder (EOS MLS) on the aura Satellite.* IEEE Transactions on Geoscience and Remote Sensing, 2006. **44**(5): p. 1075-1092.
5. Cooper, K.B., et al., *Penetrating 3-D Imaging at 4- and 25-m Range Using a Submillimeter-Wave Radar.* IEEE Transactions on Microwave Theory and Techniques, 2008. **56**(12): p. 2771-2778.
6. Wu, K., et al., *Substrate-Integrated Millimeter-Wave and Terahertz Antenna Technology.* Proceedings of the IEEE, 2012. **100**(7): p. 2219-2232.
7. Siegel, P.H., *Terahertz technology.* IEEE Transactions on Microwave Theory and Techniques, 2002. **50**(3): p. 910-928.
8. Siegel, P.H., *Terahertz technology in biology and medicine.* IEEE Transactions on Microwave Theory and Techniques, 2004. **52**(10): p. 2438-2447.
9. Nagatsuma, T., G. Ducournau, and C.C. Renaud, *Advances in terahertz communications accelerated by photonics.* Nature Photonics, 2016. **10**(6): p. 371-379.
10. Shang, X., et al., *Micromachined W-band waveguide and filter with two embedded H-plane bends.* Microwaves, Antennas & Propagation, IET, 2011. **5**: p. 334-339.
11. Zhang, M., J. Hirokawa, and M. Ando, *An E-Band Partially Corporate Feed Uniform Slot Array With Laminated Quasi Double-Layer Waveguide and Virtual PMC Terminations.* IEEE Transactions on Antennas and Propagation, 2011. **59**(5): p. 1521-1527.
12. Becker, J.P., J.R. East, and L. Katehi, *Performance of silicon micromachined waveguide at W-band.* Electronics Letters, 2002. **38**: p. 638-639.
13. Rebeiz, G.M. and G.-L. Tan, *Introduction: RF MEMS for Microwave Applications*, in *RF MEMS*. 2003. p. 1-20.
14. Pozar, D.M., *Microwave engineering*. 2011: John wiley & sons.
15. Shang, X., et al., *Micromachined W-band waveguide and filter with two embedded H-plane bends.* Iet Microwaves Antennas & Propagation, 2011. **5**: p. 334-339.
16. Li, Y., et al., *Simulation and experiment on SIW slot array antennas.* IEEE Microwave and Wireless Components Letters, 2004. **14**(9): p. 446-448.
17. Hirokawa, J. and M. Ando, *Single-layer feed waveguide consisting of posts for plane TEM wave excitation in parallel plates.* IEEE Transactions on Antennas and Propagation, 1998. **46**(5): p. 625-630.
18. Bozzi, M., et al. *On the losses in substrate integrated waveguides*. in *2007 European Microwave Conference*. 2007.
19. Feng, X. and W. Ke, *Guided-wave and leakage characteristics of substrate integrated waveguide.* IEEE Transactions on Microwave Theory and Techniques, 2005. **53**(1): p. 66-73.
20. Kildal, P., et al., *Local Metamaterial-Based Waveguides in Gaps Between Parallel Metal Plates.* IEEE Antennas and Wireless Propagation Letters, 2009. **8**: p. 84-87.
21. Kildal, P. *Three metamaterial-based gap waveguides between parallel metal plates for mm/submm waves*. in *2009 3rd European Conference on Antennas and Propagation*. 2009.
22. Beuerle, B., et al., *A Very Low Loss 220–325 GHz Silicon Micromachined Waveguide Technology.* IEEE Transactions on Terahertz Science and Technology, 2018. **8**(2): p. 248-250.
23. Malekabadi, A. and C. Paoloni, *UV-LIGA microfabrication process for sub-terahertz waveguides utilizing multiple layered SU-8 photoresist.* Journal of Micromechanics and Microengineering, 2016. **26**(9): p. 095010.
24. Shang, X., et al., *A SU8 Micromachined WR-1.5 Band Waveguide Filter.* IEEE Microwave and Wireless Components Letters, 2013. **23**(6): p. 300-302.

25. Wang, Y., et al., *Micromachined 300-GHz SU-8-Based Slotted Waveguide Antenna.* IEEE Antennas and Wireless Propagation Letters, 2011. **10**: p. 573-576.
26. Yap, M., et al. *Silicon micromachined waveguides for millimeter and submillimeter wavelengths*.
27. Rutledge, D., et al., *Antennas and waveguides for far-infrared integrated circuits.* IEEE Journal of Quantum Electronics, 1980. **16**(5): p. 508-516.
28. Becker, J.P. and L.P.B. Katehi. *Toward a novel planar circuit compatible silicon micromachined waveguide*. in *IEEE 8th Topical Meeting on Electrical Performance of Electronic Packaging (Cat. No.99TH8412)*. 1999.
29. Veidt, B., et al., *Diagonal horn integrated with micromachined waveguide for submillimetre applications.* Electronics Letters, 1995. **31**: p. 1307-1309.
30. Lee, Y., et al., *Fully micromachined finite-ground coplanar line-to-waveguide transitions for W-band applications.* IEEE Transactions on Microwave Theory and Techniques, 2004. **52**: p. 1001-1007.
31. Kirby, P.L., et al. *A micromachined 400 GHz rectangular waveguide and 3-pole bandpass filter on a silicon substrate*. in *2004 IEEE MTT-S International Microwave Symposium Digest (IEEE Cat. No.04CH37535)*. 2004.
32. Biber, S., et al., *Design and Measurement of a 600 GHz Micromachined Horn Antenna Manufactured by Combined DRIE and KOH-Etching of Silicon.* 2005.
33. Zhao, X.H., et al., *D-Band Micromachined Silicon Rectangular Waveguide Filter.* IEEE Microwave and Wireless Components Letters, 2012. **22**(5): p. 230-232.
34. Reck, T.J., et al., *Measurement of Silicon Micromachined Waveguide Components at 500–750 GHz.* IEEE Transactions on Terahertz Science and Technology, 2014. **4**(1): p. 33-38.
35. Shuang, L., et al. *WR-1.0 band waveguide band-pass filter based on micromachining technique*. in *2014 IEEE International Conference on Communiction Problem-solving*. 2014.
36. Jung-Kubiak, C., et al., *A Multistep DRIE Process for Complex Terahertz Waveguide Components.* IEEE Transactions on Terahertz Science and Technology, 2016. **6**(5): p. 690-695.
37. Shah, U., et al., *A 500–750 GHz RF MEMS Waveguide Switch.* IEEE Transactions on Terahertz Science and Technology, 2017. **7**(3): p. 326-334.
38. Reck, T., C. Jung-Kubiak, and G. Chattopadhyay, *A 700-GHz MEMS Waveguide Switch.* IEEE Transactions on Terahertz Science and Technology, 2016. **6**(4): p. 641-643.
39. Reck, T., et al., *A Silicon Micromachined Eight-Pixel Transceiver Array for Submillimeter-Wave Radar.* IEEE Transactions on Terahertz Science and Technology, 2015. **5**: p. 1-10.
40. Cegielski, P., et al., *A Four Level Silicon Microstructure Fabrication by DRIE*. 2015.
41. Rahiminejad, S., et al., *Micromachined contactless pin-flange adapter for robust high-frequency measurements.* Journal of Micromechanics and Microengineering, 2014. **24**(8): p. 084004.
42. Rahiminejad, S., et al., *Demonstration of a micromachined planar distribution network in gap waveguide technology for a linear slot array antenna at 100 GHz.* Journal of Micromechanics and Microengineering, 2016. **26**: p. 074001.
43. Rahiminejad, S., et al., *Micromachined ridge gap waveguide and resonator for millimeter-wave applications.* Sensors and Actuators A: Physical, 2012. **186**: p. 264-269.
44. Pino, M.A.-d., et al., *Micromachining for Advanced Terahertz: Interconnects and Packaging Techniques at Terahertz Frequencies.* IEEE Microwave Magazine, 2020. **21**(1): p. 18-34.
45. Mohr, J., *LIGA : A technology for fabricating microstructures and microsystems.* Sensors and Materials, 1998. **10**: p. 363-373.
46. Paoloni, C., et al., *Design and Realization Aspects of 1-THz Cascade Backward Wave Amplifier Based on Double Corrugated Waveguide.* IEEE Transactions on Electron Devices, 2013. **60**(3): p. 1236-1243.
47. Desmaris, V., et al. *Microfabrication Technology for All-Metal Sub-mm and THz Waveguide Receiver Components*. 2008.
48. Li, H., Y. Li, and J. Feng, *Fabrication of 340-GHz Folded Waveguides Using KMPR Photoresist.* IEEE Electron Device Letters, 2013. **34**(3): p. 462-464.
49. Li, H., J. Feng, and G. Bai. *Microfabrication of W-band folded waveguide slow wave structure using DRIE and UV-LIGA technology*. in *2011 IEEE International Vacuum Electronics Conference (IVEC)*. 2011.
50. Collins, C.E., et al., *A new micro-machined millimeter-wave and terahertz snap-together rectangular waveguide technology.* IEEE Microwave and Guided Wave Letters, 1999. **9**(2): p. 63-65.
51. Yang, H., et al., *WR-3 Waveguide Bandpass Filters Fabricated Using High Precision CNC Machining and SU-8 Photoresist Technology.* IEEE Transactions on Terahertz Science and Technology, 2018. **8**(1): p. 100-107.
52. Shang, X., et al., *Submillimeter wave waveguide filters fabricated by SU-8 process and laser micromachining (Review paper).* IET Microwaves, Antennas & Propagation, 2017. **11**.

53. Rahiminejad, S., et al., *SU8 ridge-gap waveguide resonator.* International Journal of Microwave and Wireless Technologies, 2014. **6**: p. 459-465.
54. Aktary, M., et al., *High-resolution pattern generation using the epoxy novolak SU-8 2000 resist by electron beam lithography.* Journal of Vacuum Science & Technology B: Microelectronics and Nanometer Structures Processing, Measurement, and Phenomena, 2003. **21**(4): p. L5-L7.
55. Vora, K.D., et al., *Specification of mechanical support structures to prevent SU-8 stiction in high aspect ratio structures.* Journal of Micromechanics and Microengineering, 2005. **15**(5): p. 978-983.
56. Lin, C.-H., et al., *A new fabrication process for ultra-thick microfluidic microstructures utilizing SU-8 photoresist.* Journal of Micromechanics and Microengineering, 2002. **12**(5): p. 590-597.
57. Carlborg, C.F., et al., *Beyond PDMS: off-stoichiometry thiol–ene (OSTE) based soft lithography for rapid prototyping of microfluidic devices.* Lab on a Chip, 2011. **11**(18): p. 3136-3147.
58. Shafagh, R.Z., W.v.d. Wijngaart, and T. Haraldsson. *NANORIM: Sub-micron structuring with reaction injection molding*. in *2017 IEEE 30th International Conference on Micro Electro Mechanical Systems (MEMS)*. 2017.
59. Rahiminejad, S., et al. *Rapid manufacturing of OSTE polymer RF-MEMS components*. in *2017 IEEE 30th International Conference on Micro Electro Mechanical Systems (MEMS)*. 2017.
60. Johnsona, D.W., et al. *SUEX Dry Film Resist@ A new Material for High Aspect Ratio Lithography*. 2012.
61. Maurischat, K., *Dry film photoresists - a never ending success story?* Circuit World, 1998. **24**(2): p. 34-37.
62. Vulto, P., et al., *Microfluidic channel fabrication in dry film resist for production and prototyping of hybrid chips.* Lab on a Chip, 2005. **5**(2): p. 158-162.
63. Ehrfeld, W., et al., *Materials of LIGA technology.* Microsystem Technologies, 1999. **5**(3): p. 105-112.
64. Lorenz, H., et al., *Low-cost technology for multilayer electroplated parts using laminated dry film resist.* Sensors and Actuators A: Physical, 1996. **53**(1): p. 364-368.
65. Kukharenka, E., et al., *Electroplating moulds using dry film thick negative photoresist.* Journal of Micromechanics and Microengineering, 2003. **13**.
66. Kildal, P., *Artificially soft and hard surfaces in electromagnetics.* IEEE Transactions on Antennas and Propagation, 1990. **38**(10): p. 1537-1544.
67. Kildal, P.-S., *Definition of Artificially Soft and Hard Surfaces for Electromagnetic Waves.* Electronics Letters, 1988. **24**: p. 168-170.
68. Silveirinha, M. and C. Fernandes, *Electromagnetic Characterization of Textured Surfaces Formed by Metallic Pins.* Antennas and Propagation, IEEE Transactions on, 2008. **56**: p. 405-415.
69. Sievenpiper, D., et al., *High-impedance electromagnetic surfaces with a forbidden frequency band.* IEEE Transactions on Microwave Theory and Techniques, 1999. **47**(11): p. 2059-2074.
70. Rajo-Iglesias, E. and P.-S. Kildal, *Numerical studies of bandwidth of parallel-plate cut-off realised by a bed of nails, corrugations and mushroom-type electromagnetic bandgap for use in gap waveguides.* Microwaves, Antennas & Propagation, IET, 2011. **5**: p. 282-289.
71. Zaman, A.U. and P.-S. Kildal, *GAP Waveguides*, in *Handbook of Antenna Technologies*, Z.N. Chen, et al., Editors. 2016, Springer Singapore: Singapore. p. 3273-3347.
72. Valero-Nogueira, A., et al., *Experimental Demonstration of Local Quasi-TEM Gap Modes in Single-Hard-Wall Waveguides.* Microwave and Wireless Components Letters, IEEE, 2009. **19**: p. 536-538.
73. Valero-Nogueira, A., et al., *Gap Waveguides Using a Suspended Strip on a Bed of Nails.* Antennas and Wireless Propagation Letters, IEEE, 2011. **10**: p. 1006-1009.
74. Zaman, A.U., et al. *Increasing parallel plate stop-band in gap waveguides using inverted pyramid-shaped nails for slot array application above 60GHz*. in *Proceedings of the 5th European Conference on Antennas and Propagation (EUCAP)*. 2011.
75. Rajo-Iglesias, E., et al., *Bed of Springs for Packaging of Microstrip Circuits in the Microwave Frequency Range.* IEEE Transactions on Components, Packaging and Manufacturing Technology, 2012. **2**(10): p. 1623-1628.
76. Rajo-Iglesias, E. and P. Kildal. *Groove gap waveguide: A rectangular waveguide between contactless metal plates enabled by parallel-plate cut-off*. in *Proceedings of the Fourth European Conference on Antennas and Propagation*. 2010.
77. Zaman, A.U., et al. *Design of transition from coaxial line to ridge gap waveguide*. in *2009 IEEE Antennas and Propagation Society International Symposium*. 2009.
78. Brazález, A.A., A.U. Zaman, and P. Kildal. *Design of a coplanar waveguide-to-ridge gap waveguide transition via capacitive coupling*. in *2012 6th European Conference on Antennas and Propagation (EUCAP)*. 2012.
79. Aljarosha, A., A.U. Zaman, and R. Maaskant, *A Wideband Contactless and Bondwire-Free MMIC to Waveguide Transition.* IEEE Microwave and Wireless Components Letters, 2017. **27**(5): p. 437-439.

80. Zaman, A.U., et al., *Design of a Simple Transition From Microstrip to Ridge Gap Waveguide Suited for MMIC and Antenna Integration.* IEEE Antennas and Wireless Propagation Letters, 2013. **12**: p. 1558-1561.
81. Nandi, U., et al., *Novel Millimeter Wave Transition From Microstrip Line to Groove Gap Waveguide for MMIC Packaging and Antenna Integration.* IEEE Microwave and Wireless Components Letters, 2017. **27**(8): p. 691-693.
82. Zaman, A.U., et al., *Novel Low-Loss Millimeter-Wave Transition From Waveguide-to-Microstrip Line Suitable for MMIC Integration and Packaging.* IEEE Microwave and Wireless Components Letters, 2017. **27**(12): p. 1098-1100.
83. Vosoogh, A., A.U. Zaman, and J. Yang. *Simple and Broadband Transition Between Rectangular Waveguide and Groove Gap Waveguide for MM-Wave Applications*. in *2018 IEEE International Symposium on Antennas and Propagation & USNC/URSI National Radio Science Meeting*. 2018.
84. Pucci, E., et al., *Study of Q-factors of ridge and groove gap waveguide resonators.* Microwaves, Antennas & Propagation, IET, 2013. **7**: p. 900-908.
85. Zarifi, D., et al., *Design and Fabrication of a High-Gain 60-GHz Corrugated Slot Antenna Array With Ridge Gap Waveguide Distribution Layer.* IEEE Transactions on Antennas and Propagation, 2016. **64**(7): p. 2905-2913.
86. Sáez, A.J., et al., *Single-Layer Cavity-Backed Slot Array Fed by Groove Gap Waveguide.* IEEE Antennas and Wireless Propagation Letters, 2016. **15**: p. 1402-1405.
87. Zaman, A.U. and P. Kildal, *Wide-Band Slot Antenna Arrays With Single-Layer Corporate-Feed Network in Ridge Gap Waveguide Technology.* IEEE Transactions on Antennas and Propagation, 2014. **62**(6): p. 2992-3001.
88. Ferrando-Rocher, M., et al., *A Dual-Polarized Slotted-Waveguide Antenna Based on Gap Waveguide Technology*. 2017.
89. Zarifi, D., A. Farahbakhsh, and A.U. Zaman, *A Gap Waveguide-Fed Wideband Patch Antenna Array for 60-GHz Applications.* IEEE Transactions on Antennas and Propagation, 2017. **65**(9): p. 4875-4879.
90. Farahbakhsh, A., D. Zarifi, and A.U. Zaman, *A mmWave Wideband Slot Array Antenna Based on Ridge Gap Waveguide With 30% Bandwidth.* IEEE Transactions on Antennas and Propagation, 2018. **66**(2): p. 1008-1013.
91. Ferrando-Rocher, M., et al., *Performance Assessment of Gap-Waveguide Array Antennas: CNC Milling Versus Three-Dimensional Printing.* IEEE Antennas and Wireless Propagation Letters, 2018. **17**: p. 2056-2060.
92. Zarifi, D., A. Farahbakhsh, and A. Zaman, *A V-Band Low Sidelobe Cavity-Backed Slot Array Antenna Based on Gap Waveguide*. 2020. 1-3.
93. Liu, J., A.U. Zaman, and J. Yang. *Two Types of High Gain Slot Array Antennas based on Ridge Gap Waveguide in the D-Band*. in *2019 IEEE-APS Topical Conference on Antennas and Propagation in Wireless Communications (APWC)*. 2019.
94. Liu, J., et al., *A Slot Array Antenna With Single-Layered Corporate-Feed Based on Ridge Gap Waveguide in the 60 GHz Band.* IEEE Transactions on Antennas and Propagation, 2019. **67**(3): p. 1650-1658.
95. Razavi, S.A., et al., *2$\times$ 2-Slot Element for 60-GHz Planar Array Antenna Realized on Two Doubled-Sided PCBs Using SIW Cavity and EBG-Type Soft Surface fed by Microstrip-Ridge Gap Waveguide.* IEEE Transactions on Antennas and Propagation, 2014. **62**(9): p. 4564-4573.
96. Pucci, E., et al., *Planar Dual-Mode Horn Array With Corporate-Feed Network in Inverted Microstrip Gap Waveguide.* IEEE Transactions on Antennas and Propagation, 2014. **62**(7): p. 3534-3542.
97. Attia, H., M.S. Sorkherizi, and A.A. Kishk. *60 GHz slot antenna array based on ridge gap waveguide technology enhanced with dielectric superstrate*. in *2015 9th European Conference on Antennas and Propagation (EuCAP)*. 2015.
98. Sorkherizi, M.S., A. Dadgarpour, and A.A. Kishk, *Planar High-efficiency Antenna Array Using New Printed Ridge Gap Waveguide Technology.* IEEE Transactions on Antennas and Propagation, 2017. **65**(7): p. 3772-3776.
99. Liu, J., et al., *Design and Fabrication of a High-Gain 60-GHz Cavity-Backed Slot Antenna Array Fed by Inverted Microstrip Gap Waveguide.* IEEE Transactions on Antennas and Propagation, 2017. **65**(4): p. 2117-2122.
100. Ahmadi, B. and A. Banai, *Direct Coupled Resonator Filters Realized by Gap Waveguide Technology.* IEEE Transactions on Microwave Theory and Techniques, 2015. **63**(10): p. 3445-3452.
101. Sorkherizi, M.S., A. Khaleghi, and P. Kildal, *Direct-Coupled Cavity Filter in Ridge Gap Waveguide.* IEEE Transactions on Components, Packaging and Manufacturing Technology, 2014. **4**(3): p. 490-495.
102. Sharifi, M. and A. Kishk, *Completely Tuned Coupled Cavity Filters in Defected Bed of Nails Cavity.* IEEE Transactions on Components, Packaging and Manufacturing Technology, 2016. **PP**: p. 1-8.

103. Alós, E.A., A.U. Zaman, and P. Kildal, *Ka-Band Gap Waveguide Coupled-Resonator Filter for Radio Link Diplexer Application.* IEEE Transactions on Components, Packaging and Manufacturing Technology, 2013. **3**(5): p. 870-879.
104. Zaman, A.U., P. Kildal, and A.A. Kishk, *Narrow-Band Microwave Filter Using High-Q Groove Gap Waveguide Resonators With Manufacturing Flexibility and No Sidewalls.* IEEE Transactions on Components, Packaging and Manufacturing Technology, 2012. **2**(11): p. 1882-1889.
105. Rezaee, M., A. Zaman, and P.-S. Kildal, *A groove gap waveguide iris filter for V-band application*. 2015. 462-465.
106. Olmo-Olmeda, A.d., et al. *A novel band-pass filter topology for millimeter-wave applications based on the groove gap waveguide*. in *2013 IEEE MTT-S International Microwave Symposium Digest (MTT)*. 2013.
107. Berenguer, A., et al. *Low insertion loss 61 GHz narrow-band filter implemented with Groove Gap Waveguides*. in *2014 44th European Microwave Conference*. 2014.
108. Sun, D. and J. Xu, *A Novel Iris Waveguide Bandpass Filter Using Air Gapped Waveguide Technology.* IEEE Microwave and Wireless Components Letters, 2016. **26**(7): p. 475-477.
109. Al-Juboori, B., et al. *Millimeter wave cross-coupled bandpass filter based on groove gap waveguide technology*. in *2017 10th UK-Europe-China Workshop on Millimetre Waves and Terahertz Technologies (UCMMT)*. 2017.
110. Sorkherizi, M.S. and A.A. Kishk, *Self-Packaged, Low-Loss, Planar Bandpass Filters for Millimeter-Wave Application Based on Printed Gap Waveguide Technology.* IEEE Transactions on Components, Packaging and Manufacturing Technology, 2017. **7**(9): p. 1419-1431.
111. Vosoogh, A., A.A. Brazález, and P. Kildal, *A V-Band Inverted Microstrip Gap Waveguide End-Coupled Bandpass Filter.* IEEE Microwave and Wireless Components Letters, 2016. **26**(4): p. 261-263.
112. Sorkherizi, M.S. and A.A. Kishk, *Fully Printed Gap Waveguide With Facilitated Design Properties.* IEEE Microwave and Wireless Components Letters, 2016. **26**(9): p. 657-659.
113. Rezaee, M. and A. Zaman, *Groove Gap Waveguide Filter Based on Horizontally Polarized Resonators for V-Band Applications.* IEEE Transactions on Microwave Theory and Techniques, 2020. **PP**: p. 1-1.
114. Rajo-Iglesias, E., A. Zaman, and P.-S. Kildal, *Parallel Plate Cavity Mode Suppression in Microstrip Circuit Packages Using a Lid of Nails.* Microwave and Wireless Components Letters, IEEE, 2010. **20**: p. 31-33.
115. Zaman, A.U., J. Yang, and P. Kildal. *Using Lid of pins for packaging of microstrip board for descrambling the ports of eleven antenna for radio telescope applications*. in *2010 IEEE Antennas and Propagation Society International Symposium*. 2010.
116. Brazalez, A.A., A.U. Zaman, and P. Kildal, *Improved Microstrip Filters Using PMC Packaging by Lid of Nails.* IEEE Transactions on Components, Packaging and Manufacturing Technology, 2012. **2**(7): p. 1075-1084.
117. Vosoogh, A., et al., *Compact Integrated Full-Duplex Gap Waveguide-Based Radio Front End For Multi-Gbit/s Point-to-Point Backhaul Links at E-Band.* IEEE Transactions on Microwave Theory and Techniques, 2019. **67**(9): p. 3783-3797.